5-2013

Live-Load Test and Finite-Model Analysis of an Integral Abutment Concrete Girder Bridge

Robert W. Fausett
Utah State University

LIVE-LOAD TEST AND FINITE-ELEMENT MODEL ANALYSIS OF AN INTEGRAL ABUTMENT CONCRETE GIRDER BRIDGE

by

Robert W. Fausett

A thesis submitted in partial fulfillment
of the requirements for the degree

of

MASTER OF SCIENCE

in

Civil and Environmental Engineering

Approved:

_____	_____
Dr. Paul J. Barr Major Professor	Dr. Joseph A. Caliendo Committee Member
_____	_____
Dr. Marvin W. Halling Committee Member	Dr. Mark R. McLellan Vice President for Research and Dean of the School of Graduate Studies

UTAH STATE UNIVERSITY
Logan, Utah

2013

ABSTRACT

Live-Load Test and Finite-Element Model Analysis of an

Integral Abutment Concrete Girder Bridge

by

Robert W. Fausett, Master of Science

Utah State University, 2013

Major Professor: Dr. Paul J. Barr
Department: Civil and Environmental Engineering

As part of the Long Term Bridge Performance (LTBP) Program, a single-span, prestressed, integral abutment concrete girder pilot bridge near Perry, Utah was instrumented with strain gauges, deflectometers, and temperature gauges at various locations onto the bridge for long-term monitoring and periodic testing. One of the periodic tests conducted on this bridge was a live-load test. The live-load test included driving trucks across the bridge, as well as parking trucks along different lanes of the bridge, and measuring the deflection and strain. The data collected from these sensors was used to create and calibrate a finite-element model (FEM) of the bridge. The model was afforded the same dimensions and characteristics as the actual bridge, and then the boundary conditions were altered until the FEM data and live-load data showed a strong correlation. Live-load distribution factors and load ratings were then obtained using this calibrated model and compared to the AASHTO LRFD Bridge Design Specifications. The results indicated that in all cases, the AASHTO LRFD Specification distribution factors were conservative by between 55% to 78% due to neglecting to take the bridge

fixity (bridge supports) into account in the distribution factor equations. The actual fixity of the bridge was determined to be 94%.

Subsequently, a parametric study was conducted by creating new models based on the original bridge for changes in span length, deck thickness, edge distance, skew, and fixity to determine how different variables affect the bridge. Distribution factors were then calculated for each case and compared with the distribution factors obtained from the AASHTO LRFD Specifications for each case. The results showed that the variables with the largest influence on the bridge were the change in fixity and the change in skew. Both parameters provided ranges between 10% non-conservative and 56% conservative. The parameter with the least amount of influence was the deck thickness providing a range between 4% non-conservative and 19% non-conservative. Depending on which variable was increased, both increases and decreases in conservatism were exhibited in the study.

(87 pages)

PUBLIC ABSTRACT

Live-Load Test and Finite-Element Model Analysis of an

Integral Abutment Concrete Girder Bridge

by

Robert W. Fausett, Master of Science

Utah State University, 2013

Major Professor: Dr. Paul J. Barr
Department: Civil and Environmental Engineering

As part of the Long Term Bridge Performance (LTBP) Program, a single-span, prestressed, integral abutment concrete girder pilot bridge near Perry, Utah was instrumented with different sensors at various locations onto the bridge for long-term monitoring and periodic testing. One of the periodic tests conducted on this bridge was a live-load test. The live-load test included driving trucks across the bridge, as well as parking trucks along different lanes of the bridge, and measuring the deflection and strain. The data collected from these tests was used to create and calibrate a computer model of the bridge. The model was afforded the same dimensions and characteristics as the actual bridge, and then the boundary conditions (how the bridge is being supported) were altered until the model data and the live-load data matched. Live-load distribution factors and load ratings were then obtained using this calibrated model and compared to the AASHTO LRFD Bridge Design Specifications. The results indicated that in all cases, the AASHTO LRFD Specification distribution factors were conservative by between 55% to 78% due to neglecting to take the bridge fixity (bridge supports) into

account in the distribution factor equations. The actual fixity of the bridge was determined to be 94%.

Subsequently, a variable study was conducted by creating new models based on the original bridge for changes in span length, deck thickness, edge distance, skew (angle of distortion of the bridge), and fixity to see how each variable would affect the bridge. Distribution factors were then calculated for each case and compared with the distribution factors obtained from the AASHTO LRFD Specifications for each case. The results showed that the variables with the largest influence on the bridge were the change in fixity and the change in skew. Both parameters provided ranges between 10% non-conservative and 56% conservative. The parameter with the least amount of influence was the deck thickness providing a range between 4% non-conservative and 19% non-conservative. Depending on which variable was increased, both increases and decreases in conservatism were exhibited in the study.

Robert W. Fausett

ACKNOWLEDGMENTS

I would like to thank all of the people in my life that lifted me up and have allowed me to excel to the point that I am today. I would also like to thank all of the people in my life without whom I would never have been able to accomplish this grand feat. First, and foremost, I would like to thank my wife who put up with my incessant studying and never ending late nights. Without her, I would not have been able to keep motivated to finish. She is the perfect wife and the perfect woman.

I would like to thank all of my professors and past school teachers who have pushed me along the way throughout my school careers and have had to put up with my hilarious jokes and indelible good looks. Special thanks to Dr. Barr, Dr. Halling, and Dr. Joe who have worked with me and taught me things far and above what was required of them, and for that I am ineffaceably indebted. All are forevermore my friends.

I would like to thank my parents (all of them) and siblings, for everything they have done for me including instilling an ineradicable tenacity with which I have encountered and faced all of my toughest challenges head on. Without them and their love and support, I surely would not be the Man I am today.

Finally, I would like to thank my friends; if not for the inexpugnable accelerated velocity of the terminological inexactitude that they have fed me for all of my years in school, I would not have had the confidence to pursue my greatest achievements in life thus far.

Just a quick shout out to my future dog, he/she is going to be inextricably cherubic in its enduring resplendency. Thank you again to everyone.

Bobby Fausett

CONTENTS

Page

LIST OF TABLES

LIST OF FIGURES

LIST OF EQUATIONS

CHAPTER 1

INTRODUCTION

The Long Term Bridge Performance (LTBP) Program is a 20-year long project with the goals to create a comprehensive database of a sample number of bridges that will be tested in order to predict the current and future states of the bridges in the United States. These test bridges have been selected from a variety of bridge types across the United States based on how well they represent U.S. bridges and on how much could be learned from the bridges. On each of these bridges, different tests have been and are continuing to be conducted. Through the implementation of these tests, a broader knowledge and understanding has been gained of how bridges experience corrosion, flaws, fatigue, environmental elements, and cyclical vehicle loading. Through this additional knowledge, the design of new bridges and the maintenance of current and future bridges will be improved.

Integral bridges have been employed since 1938 when the Teens Run Bridge was constructed near Eureka, Ohio. Integral bridges can be either single-span or continuous multiple-span bridges without movable transverse deck joints at the piers or abutments. This design subjects the superstructure and abutment to secondary stresses due to the continuity of the bridge when the bridge settles and is backfilled. Although these stresses are not ideal, the damage and distress found to be caused by having movable deck joints is much more significant than the damage and distress occurring from the secondary stresses these joints are intended to prevent (Burke 2009). Across the United States, more and more DOTs are using these integral abutment designs, however, the current

code does not provide any relief for this fixed-fixed support and requires that these bridges to be designed to simple-support standards.

Finite-element analysis has been a practical tool utilized in many studies of integral abutment bridges. The model created provides an accurate representation of the actual bridge which can then be manipulated using different loads and bridge characteristics to quantify different bridge response. In previous studies, a finite-element model has been created either as a replication of an actual bridge, or as a representation of a general bridge of a certain type (i.e. integral abutment, box girder). In all of these studies, the finite-element model was loaded similarly to traffic travelling across the bridge and the overall performance of the bridge, as well as the distribution factors and load ratings, were determined. Examples of these studies include Barr et al. (2001), Mourad and Tabsh (1999), Dicleli and Erhan (2009), Hodson et al. (2012), Lahovich (2012), and Kalayci et al. (2011).

Although many integral abutment bridge studies have been conducted using finite-element models, integral abutment bridges have not been as readily studied when it comes to calibrated models. Live-Load Distribution Factors (LLDF)s have been found for integral abutment bridges using theoretical bridge models such as Dicleli and Erhan, which studied live-load distribution formulas for single-span prestressed concrete integral abutment bridge girders, Mourad and Tabsh, which studied deck slab stresses in integral abutment bridges using two separate bridge models differing in beam cross sections, slab thicknesses, and number of spacing piles, and Lahovich, whom came up with live-load distribution factors for an integral abutment bridge, a “bridge in a backpack,” and the folded plate girder bridge in order to determine how each of the bridges behaved under

various types of loading. LLDFs have also been found for other types of bridges using calibrated finite-element models based on actual bridges such as studies conducted by Barr et al. (2001) and Hodson et al. (2012) for a three-span, concrete girder bridge and cast-in-place, box girder bridge, respectively. Kalayci et. al. (2011) also use a calibrated finite-element model in order to determine the LLDFs of two integral abutment bridges in Vermont, though these bridges were composite with concrete decks and steel I-girders and will behave differently than a bridge comprised of concrete girders. While single span integral abutment bridges are the most frequent type, few studies have been performed using finite-element models calibrated from live-load test data on a single-span, prestressed, integral abutment concrete girder bridge to determine LLDFs.

As part of the LTBP Program, Utah State University, in cooperation with the Federal Highway Administration (FHWA), Rutgers University, and the Utah Department of Transportation (UDOT), instrumented sensors on a single-span, prestressed, integral abutment concrete girder pilot bridge near Perry, Utah, for long-term monitoring and periodic testing. One of the periodic tests conducted on this bridge was a live-load test. The setup of this test involved attaching strain gauges, deflectometers, and temperature gauges at various locations onto the bridge. The live-load test included driving trucks across the bridge, as well as parking trucks along different lanes of the bridge. The data collected from these tests was used to create and calibrate a finite-element model (FEM) of the bridge. The model was afforded the same dimensions and characteristics as the actual bridge, and then the boundary conditions were altered until the FEM data and live-load data showed a strong correlation. Live-load distribution factors and load ratings were then obtained using this calibrated model and compared to the AASHTO LRFD

Bridge Design Specifications. The results indicated that in all cases the AASHTO LRFD Specification distribution factors were overly conservative, between 55% and 78%, due to neglecting to take the fixity of the bridge ends into account in the distribution factor equations. When the FEM was compared to a completely stiff moment, the distribution factors fell within a range of 8% non-conservative and 47% conservative. This shows the bridge is likely in between the two extremes of fixity.

Subsequently, a parametric study was conducted by creating new models based on the original bridge for changes in span length, deck thickness, edge distance, skew, and fixity to determine how different variables affect the bridge. Distribution factors were then calculated for each case and compared with the distribution factors obtained from the AASHTO LRFD Specifications for each case. The results showed that the variables with the largest influence on the bridge were the change in fixity and the change in skew. Both parameters provided ranges between 10% non-conservative and 56% conservative. The parameter with the least amount of influence was the deck thickness providing a range between 4% non-conservative and 19% non-conservative. Depending on which variable was increased, both increases and decreases in conservatism were exhibited in the study.

CHAPTER 2

PRELITERATURE REVIEW

2.1 Live-Load Distribution Factors in Prestressed Concrete Girder Bridges (Barr et al. 2001)

The research presented in this article focused on determining flexural live-load distribution factors for three-span, prestressed concrete girder bridges. The study used the results from a live-load test on a bridge in Washington in order to calibrate 24 finite-element models which then were used to obtain Live-Load Distribution Factors (LLDFs). The moments calculated from the recorded strain values of the actual bridge, as compared to the moments computed from the finite-element model, differed by a maximum of less than 6% showing a good correlation.

Changes in LLDFs due to lifts, intermediate diaphragms, end diaphragms, continuity, skew angle, and load types were determined by comparing the finite-element model of the Washington Bridge to alternative models with adjusted characteristics. The study also compared the acquired LLDFs to those calculated in accordance to the American Association of State Highway and Transportation Officials (AASHTO) Load and Resistance Factor Design (LRFD) Specifications. When making this comparison, the study found that the AASHTO LRFD procedures were up to 28% larger than the calculated LLDFs from the finite-element models, meaning the AASHTO LRFD specifications are relatively conservative. However, this large percentage difference occurred when comparing the alternative bridge models such as imposing lifts and different skew angles. When comparing the models that most closely followed the configuration that was considered in developing the LRFD specifications to the LRFD specifications, the distribution factors varied by a maximum of 6%.

The final conclusions of the paper indicate that distribution factors decrease with an increase in skew, distribution factors calculated for lane loading are lower than those calculated for truck loading, and finally, if the Washington Bridge used in the study had been designed using finite-element model analysis, the required release strength could have been reduced by 1000 psi (6.9 MPA) or the bridge could have been designed for a 39% higher live-load.

2.2 Live-Load Analysis of Posttensioned Box-Girder Bridges (Hodson et al. 2012)

This study focused on the determination of flexural live-load distribution factors for cast-in-place, box-girder bridges. The bridge used for this research was a two-span, cast-in-place, prestressed, continuous box-girder bridge with a skew of 8˚. This bridge was instrumented with 42 uniaxial strain transducers (strain gauges), 10 vertical deflection sensors (displacement transducers), and one uniaxial rotation sensor (tilt sensor). A live-load test was conducted by driving two heavily loaded trucks along predetermined load paths of the bridge. The data collected from the live-load test was then used to calibrate a finite-element model of the bridge. Once calibrated, the finite-element model was then used to determine the actual live-load distribution factors and load ratings for the bridge. These values were compared to the distribution factors and ratings in accordance to the AASHTO LRFD Specifications. In addition, the finite-element model was used to investigate the various bridge parameters affecting the distribution of vehicle loads for this type of bridge.

The parameters evaluated included span length, girder spacing, parapets, skew, and deck thickness. This study concluded that the procedures to calculate the distribution factors from the AASHTO LRFD Specifications are conservative as compared to the

finite-element model distribution factors for the interior girder. Additionally, the AASHTO LRFD Specifications are non-conservative for the exterior girder distribution factors. In response to these findings, and through the use of the relationships obtained through the parametric study, a new equation for calculating exterior girder distribution factors was proposed to ensure a more conservative approach.

2.3 Live Load Distribution Formulas for Single-Span Prestressed Concrete Integral Abutment Bridge Girders (Dicleli and Erhan 2009)

The research presented in this article focused on determining formulas for live-load distribution factors for the girders of a single-span integral abutment bridge. To accomplish this objective, the researchers developed two and three dimensional finite-element models of multiple different integral abutment bridge types. The study used a variation of the bridge model's superstructure in order to improve the current understanding of integral abutment bridges. The bridge properties that were varied included span length, number of design lanes, prestressed concrete girder size and spacing, and slab thickness.

Live-load distribution factors (LLDFs) were determined using the different models and then these values were compared to the LLDFs calculated in accordance with the American Association of State Highway and Transportation Officials (AASHTO) Specifications for simply supported bridges. In comparison to the AASHTO Specifications, the determined formulas for the interior girder shear differed by as much as 10%, but were generally between 3-6%. For the girder moments and outside girder shear, the results varied greatly. Some comparisons provided nearly exact matches between the models and AASHTO Specifications while other results varied by as much

as 87%. Generally these results were conservative, however, there were cases where the comparisons were up to 13% non-conservative.

The results of this study led the researchers to conclude that the AASHTO Specifications for simply supported bridges could be used for interior girder shear but was inaccurate for girder moments or outside girder shear due to the large variations. Modifications were provided by the authors for the AASHTO LLDF Specifications which, the authors state, will provide more accurate LLDFs for IABs. In addition to those modifications, other equations were provided and determined to provide good results independent of the AASHTO LLDF Specifications.

2.4 Deck Slab Stresses in Integral-abutment Bridges (Mourad and Tabsh 1999)

The research presented in this article involved using finite-element models to evaluate the behavior of integral-abutment bridges with concrete deck slabs on composite steel beams. The results of these models were then compared to the American Association of State Highway and Transportation Officials (AASHTO) Specifications. This study was performed in response to integral-abutment bridges being built using the design specifications provided by AASHTO for jointed bridges without regard to the different behavior of the integral-abutments.

Two integral-abutment bridges were modeled in this study differing in slab thickness, beam cross sections, and the number of spacing piles. The load for the models consisted of two HS20 trucks placed side-by-side in accordance with the 1996 AASHTO Load Factor Design provisions. The moments provided from the models were then compared to simply supported bridges of equal size and similar properties. In addition,

the stresses presented by the model were compared to the stresses calculated using the AASHTO Specifications for bridges.

When comparing the moments, the researchers determined that the maximum positive moment in the deck slabs was 10-30% lower for the integral-abutment bridges as compared to the simply-supported bridges. The differences nearly doubled for the case of negative moments with the integral-abutment bridges being 20-70% lower than the simply-supported bridges. When comparing the stresses from the finite-element models to the AASHTO Specifications, the study concludes that the integral-abutment bridges are conservative by 40%.

2.5 New Technologies in Short Span Bridges: A Study of Three Innovative Systems (Lahovich 2012)

The research presented in this paper involved studying the behavior of three separate types of short span bridges: integral abutment bridges, "bridge-in-a-backpack", and the folded plate girder bridge. The "bridge-in-a-backpack" and folded plate girder bridges were studies performed on actual bridges. These bridges were instrumented throughout construction and live-load tests were conducted on them upon their completion. The author concluded that the largest strains for both bridges were experienced during the construction of the bridges. The bridges were continually monitored for long-term effects until the end of 2011, and the study ended due to issues with the data acquisition system.

The author created detailed finite-element models for different theoretical integral abutment bridges. This analytical study was performed by varying the span lengths, skew angles, and beginning or not beginning the live-load analysis from the stiffness of the deformed shape under active soil pressure and dead load. This study also included

the analysis of simply supported bridge models with similar characteristics, and then determined the live-load distribution factors for the integral abutment bridge models. These LLDFs were then compared to the distribution factors calculated in accordance to the procedure in the AASHTO LRFD specifications to determine whether or not the design of integral abutment bridges using common practices is conservative.

The conclusions obtained from this study were that the midspan moments for the integral abutment bridge models were between 35-50% less than those from the model with the simply supported models. The author concludes that if an engineer designs for the simply-supported structure, that moment could be up to 50% greater than the moment actually experienced in an integral abutment bridge.

When comparing the live-load distribution factors to the AASHTO LRFD equations, the author determined that the LLDFs increased as the skew angle was increased, while the AASHTO LRFD skew correction factor reduces the LLDFs under the same conditions. Similar to the finite-element comparison, the author concluded that the design of integral abutment bridges was conservative when designed assuming simply supported conditions.

The effect of initiating the analysis from the stiffness, based on the deformed shape under active earth pressure and dead load, was determined to have the largest effect for long spans with higher skews. The author concluded that a maximum increase of less than 5% for the LLDFs for the midspan moment, a maximum decrease in the LLDFs of the endspan moments of 10%, and no effect for the shear LLDFs occurred when beginning the analysis based on the deformed shape, rather than the undeformed shape.

2.6 Load Testing and Modeling of Two Integral Abutment Bridges in Vermont, US (Kalayci et al. 2011)

The research presented in this article focused on comparing two integral abutment bridges (IABs), located in Vermont, US, with two finite-element models (FEMs) and live-load test data. Both bridges were designed using composite steel I-girders with reinforced concrete decking, HP piles, wing walls, and abutments. The two bridges spanned 43 m (141 ft) and 37 m (121 ft) long. For the live-load test, each bridge was instrumented with displacement transducers, tilt meters, earth pressure cells, strain gauges, and inclinometers. These gauges measured changes in the overall movement, earth pressure against the abutment, the strain of the girders, as well as the strain and angle of the piles. In addition, each gauge was equipped with a thermistor to record the temperature at the gauge location. For the live-load test, each bridge was loaded with either two or three loaded dump trucks stationed at 13 various positions across the bridges.

After the live-load test of each bridge, the data was analyzed and it was determined that temperature corrections were required for the measured data in order to determine accurate neutral axis locations for the girder cross sections. Finite-element models were created in order to replicate each of the bridges. Once created, these FEMs were calibrated to more accurately represent each of the bridges. The research concluded that the superstructure of the two IABs had a 20% higher negative moment at the ends, when taken as an absolute value, as compared with the positive bending moment at the midspan. The researchers also concluded that the substructure displacements were minimal for both bridges and the backfill pressures were negligible due to winter month temperatures. Overall, the researchers suggest that temperature induced stress is a

problem and should be taken into account, and that live-load distribution factors would provide more beneficial information.

CHAPTER 3

BRIDGE DESCRIPTION

The Utah Pilot Bridge (structure number 1F 205), as shown in Fig. 1, was selected as part of a larger study of bridge performance for the Long Term Bridge Performance Project (LTBP). The research conducted was performed by Utah State University. The structure, constructed in 1976, is a single span, five girder, pre-stressed concrete bridge built with integral abutments. It is located 80.5 km (50 miles) north of Salt Lake City, UT. The bridge carries two lanes of northbound traffic, as part of Interstate 15/84 traveling over Cannery Road in the town of Perry, UT. The exact location is 41° 27' 25.92" latitude and 112° 03' 18.72" longitude. The bridge has a clear span length of 24.4 m (80 ft) and an overall length of 25.1 m (82.5 ft). The height from the road below is 4.68 m (15.34 ft). Fig. 2 shows a cross section of the bridge. The bridge incurs an average daily traffic (ADT) of approximately 22,000 vehicles, 29 percent of which are large trucks. There is no skew associated with this bridge. A superelevation of 2% was built into the bridge.

The width of the deck is 13.5 m (44.4 ft) long measured from the outside of the barriers, and 12.3 m (40.5 ft) long measured from the inside of the barriers. The deck is comprised of 203 mm (8 in.) thick of reinforced concrete with a 152 to 203 mm (6 to 8 in.) asphalt overlay. The concrete had a specified compressive strength of 24.1 MPa (3500 psi) and was reinforced with Grade 60 billet-steel, size 5 bars with at least a 50.8 mm (2 in.) cover. A cross section of the deck is shown in Fig. 3. The barriers were cast with a cold joint and have a height of 1.07 m (3.5 ft) running along either side of the bridge. The barriers are reinforced with size 4 bars of Grade 60 steel with a cover of at least 38.1 mm (1.5 in.).

Fig. 1 Utah Pilot Bridge (structure number 1F 205) side view

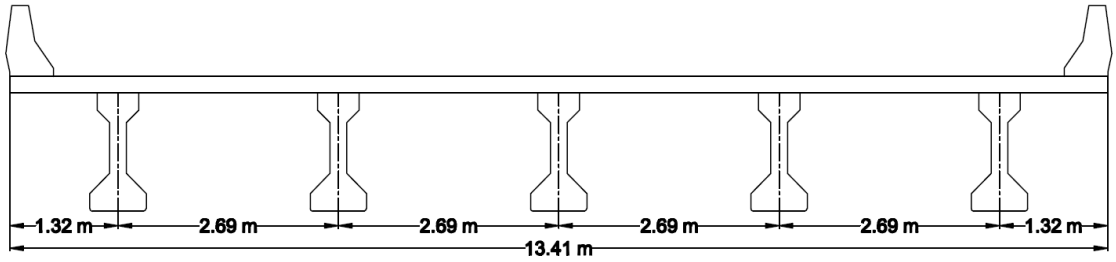

Fig. 2 Utah Pilot Bridge cross section

The girders supporting the deck are precast AASHTO Type IV bridge girders and are 25.1 m (82.5 ft) long, 1.37 m (4.5 ft) tall, and made of precast concrete. A cross section of the girder is shown in Fig. 4. The specified compressive strength of the

concrete was 34.5 MPa (5000 psi) and was reinforced with Grade 60 steel. The girder was prestressed prior to shipping to the job site using a harped strand profile. The harping points are located 9.75 m (32 ft) from the ends of the girder on either side and the centroid of the strands at this point is 103 mm (4.06 in.) from the bottom of the girders. At the girder ends, the centroid of the strands is located at 340 mm (13.4 in.) from the bottom of the girders. The final prestressing force for each girder, after losses, was estimated to be 3367 kN (757 kips). The girders have a center-to-center spacing of 2.68 m (8.8 ft).

The support of the Utah Pilot Bridge superstructure is comprised of integral abutments that are 0.76 m (2.5 ft) thick and 3.20 m (10.5 ft) tall and span the width of the bridge. Within the abutment, each girder rests on a 12.7 mm (0.5 in.) elastomeric bearing pad. These pads are above 76.2 mm (3 in.) tall concrete pedestals which transfer the load from the girders to five concrete drilled piles which each have a maximum allowable load of 356 kN (80 kips). Wing walls were cast adjacent to both abutment ends and are positioned parallel to the bridge with a total length of 4.72 m (15.5 ft), a width of 0.30 m (1 ft), a height of 2.90 m (9.5 ft) near the abutment, and a height of 0.61 m (2 ft) near the center of the bridge.

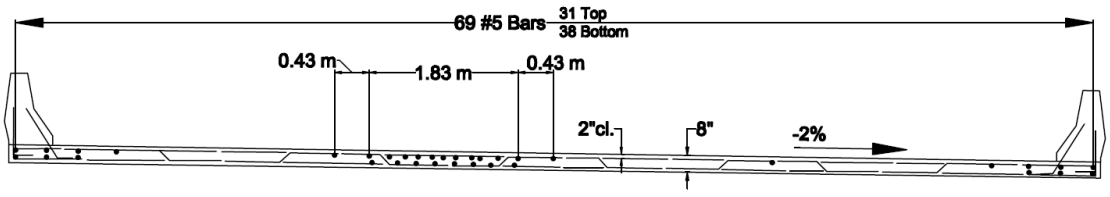

Fig. 3 Utah Pilot Bridge deck cross section

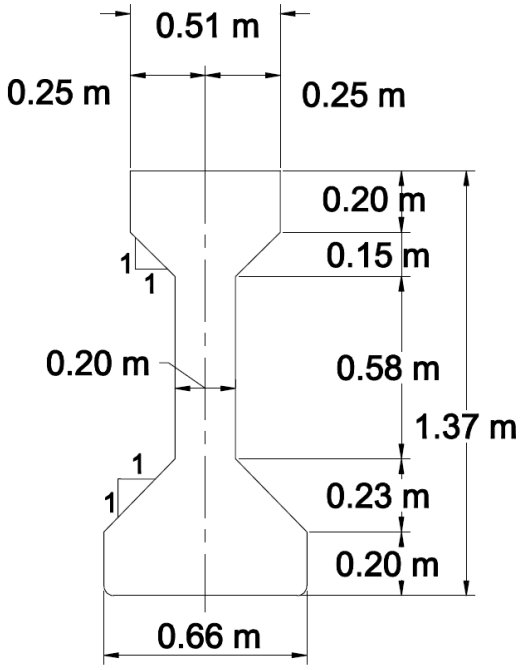

Fig. 4 Utah pilot bridge girder cross section

Inspections and repairs have occurred on this bridge while it has been in service. In September of 1982, an inspection report for the bridge mentioned severe wear and dilapidation. In September of 1991, the deck surface and parapets were repaired due to findings in the 1982 report. An inspection taking place in 1995 reported that the repairs were complete and looked good. In 1997, the inspection report made mention of minor cracking with efflorescence at the south end of the bridge. In 2005, a new asphalt overlay was placed on the deck after reports that the cracking had gotten much worse since the 2003 inspection report. The 2005 inspection also recorded spalling in the parapets along with full transverse cracking with efflorescence every 1.52 to 2.13 m (5 to 7 ft). Finally, a report in 2010, despite giving the bridge a 95.1 sufficiency rating, recommended the replacement of the bridge due to substandard load carrying capacity or inadequate bridge roadway geometry. This replacement had an estimated cost of $515,000.

CHAPTER 4

EXPERIMENTATION

4.1 Instrumentation

The live-load test was conducted by driving a truck or combination of trucks along a predetermined load path and measuring the strain, displacement, and temperature from sensors that were installed on the bridge. The sensors installed on the structure are positioned in four separate locations longitudinally along the bridge. These sensors include twenty surface mounted strain sensors, as shown in Fig. 5, and seven deflectometer vertical displacement sensors, as shown in Fig. 6. Most instruments were mounted using a boom lift though the instruments near the abutment were reached using the embankment underneath the bridge. Researchers used a fast setting adhesive and specially designed mounting tabs in order to fasten the instruments to the concrete. The

Fig. 5 Surface mounted strain transducer

Fig. 6 Deflection instrument, "deflectometer”

deflectometers were deflected before the live-load test using a weight located on the ground to hold the deflection.

The strain sensors were placed in two locations horizontally across the bridge; one set at 13.1 m (43 ft) and the other set at 22.9 m (75 ft) as measured from the south end of the bridge. These locations are marked as cross sections BB and DD in Fig. 7. In theory, the ideal locations for the sensors would be at the abutment and at the mid-span. Due to the harping point and diaphragm at the mid-span, gauge locations where slightly adjusted. In addition, placing a strain gauge right on the abutment would provide for extremely low strain readings. In order to receive accurate and useable data, the gauges were offset by 0.91 m (3 ft) from the mid-span and 1.52 m from the abutment. The strain sensors were also placed at two different locations along the height of the girder. Half of the

instruments were placed on the bottom flange of the girders while the other half were placed near the top of the web of the girders. The locations of the sensors at cross sections BB and DD, as well as the sensor identification numbers, are provided in Fig. 8 and Fig. 9, respectively.

Like the strain sensors, the deflection sensors were also split between two longitudinal locations, however, for these sensors, five were placed in one longitudinal location while only two were placed in the other location. These two locations are shown as cross sections AA and CC, respectively, in Fig. 7. Because the harping point and diaphragm would have no effect on the deflectometers, the set of five deflection sensors was put at the exact mid-span of 12.2 m (40 ft). This is cross section AA and can be seen in Fig. 10. The other two deflectometers were placed at 14.6 m (48 ft) as measured from the south end of the bridge. This point was cross section CC of the bridge and is provided as Fig. 11. All of the deflectometers were attached on the bottom flange of the girders.

4.2 Live-Load Paths

Multiple live-load tests were performed using a controlled lane closure during a time of low traffic flow. In addition, a moving roadway block was utilized in order to keep all traffic off the bridge during testing. This was accomplished by having a highway patrol car drive down the middle of both lanes of the highway, beginning 3.66 km (2.28 miles) before the bridge, in order to cause a slowdown in traffic, as shown in Fig. 12. This slowdown allowed for a window of four to five minutes of uninterrupted testing. In this amount of time, trucks were positioned and one load path was able to be completed.

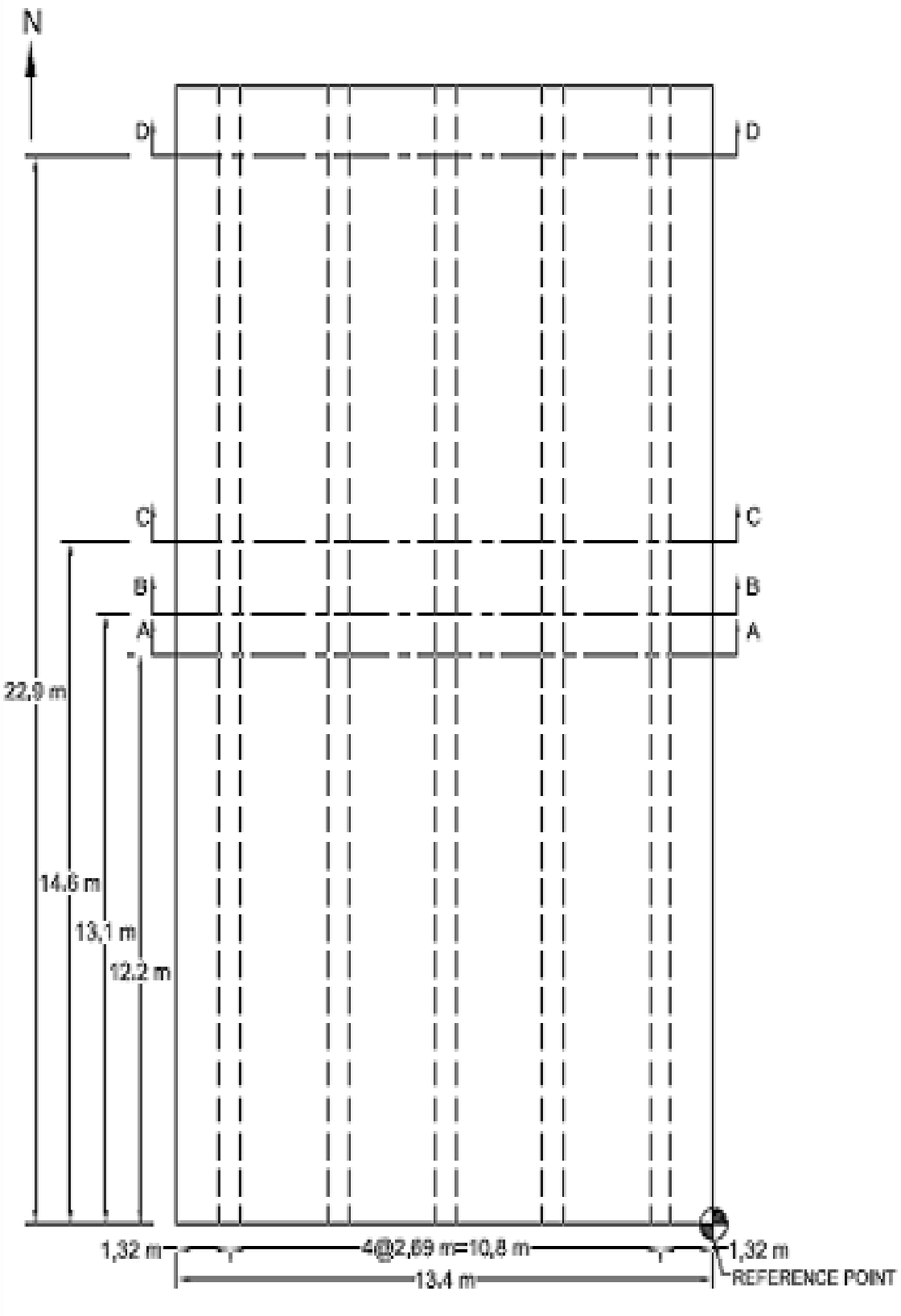

Fig. 7 Plan view of bridge providing instrumentation locations

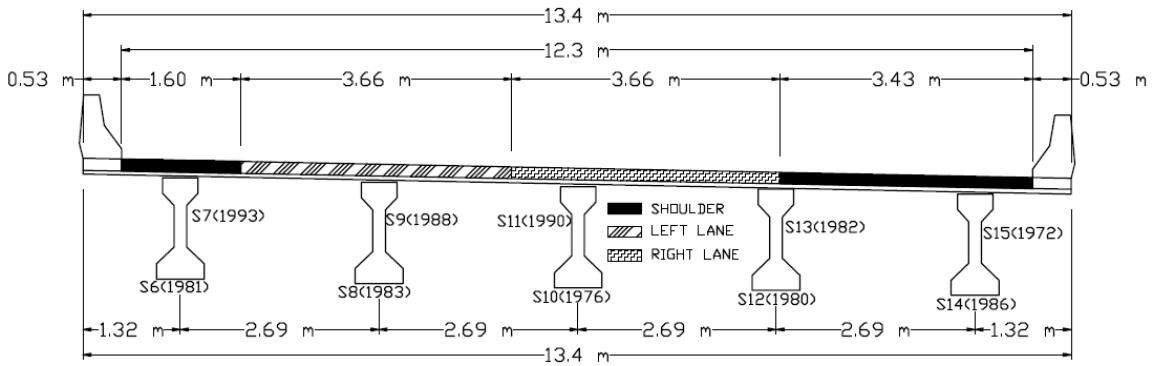

Fig. 8 Bridge cross-sectional view Section B-B

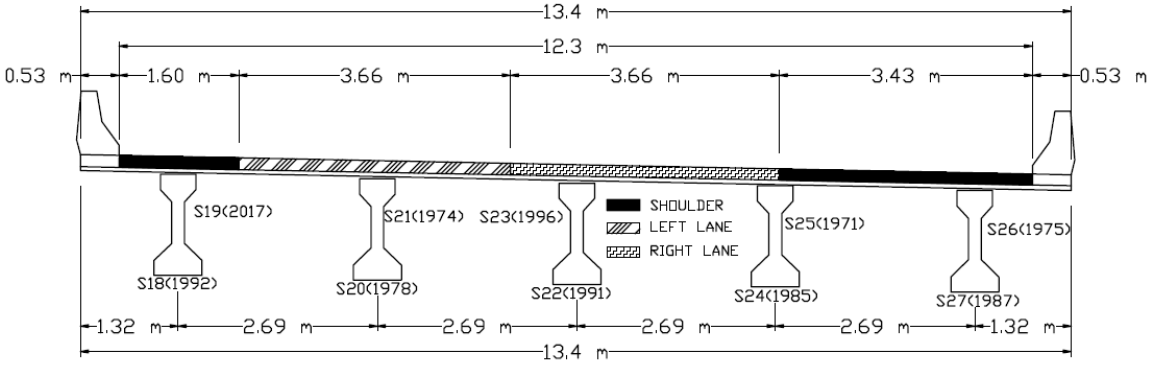

Fig. 9 Bridge cross-sectional view Section D-D

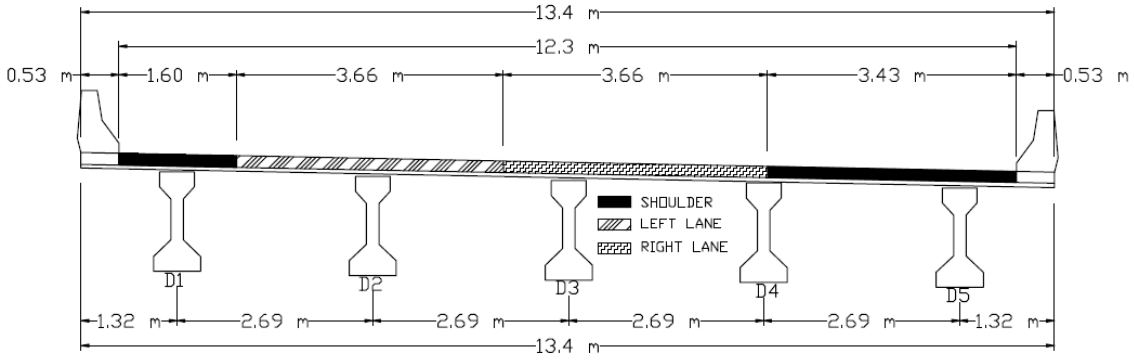

Fig. 10 Bridge cross-sectional view Section A-A

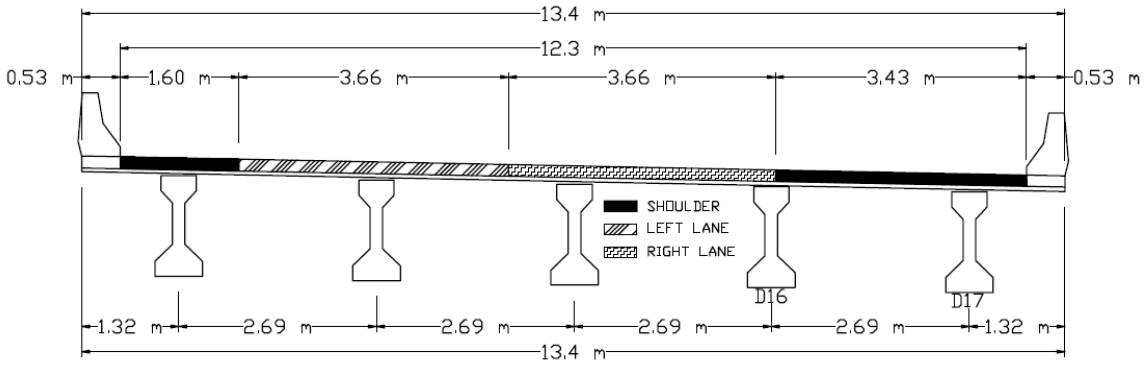

Fig. 11 Bridge cross-sectional view Section C-C

Two heavily loaded UDOT tandem rear axle dump trucks were used to apply the live-load weights. Truck A had a Gross Vehicle Weight (GVW) of 223 kN (50,080 lbs) while Truck B had a GVW of 229 kN (51,460 lbs). Both trucks are shown in Fig. 13. All Truck A and Truck B information is provided in Table 1 and Table 2, respectively. Fig. 14 and Fig. 15 provide dimensions of the footprints of Truck A and Truck B, respectively. Six tests were conducted in all, one high speed test and five pseudo-static tests (truck driving at 5 mph). The strains, displacements, and corresponding truck positions were both recorded at a frequency of 100 Hz for the high speed test and 50 Hz for the pseudo-static tests. The load cases describe the six different tests that occurred during the live-load testing. Table 3 provides information for the different load cases. The load paths are the positions the trucks are either placed at or, in the case of the high speed test, the part of the bridge the truck drove over. Information regarding the load paths can be found in Table 4. In order to show details of each of the load cases, Fig. 16 through Fig. 19 are provided.

The truck position was monitored for the first five load cases using a device called an "Autoclicker" which was mounted to the driver side tire of Truck A, at each wheel

Fig. 12 Police officers causing a slowdown in traffic.

Fig. 13 Truck A and Truck B

Table 1 Truck A information

Axle	Spacing (m)	Gauge (m)	Weight (kg)
1	-	2.03	7,756
2	4.11	1.88	7,480
3	1.35	1.88	7,480
		Total	22,716

Table 2 Truck B information

Axle	Spacing	Gauge	Weight (kg)
1	-	2.03	7,747
2	4.09	1.88	7,797
3	1.37	1.88	7,797
		Total	23,342

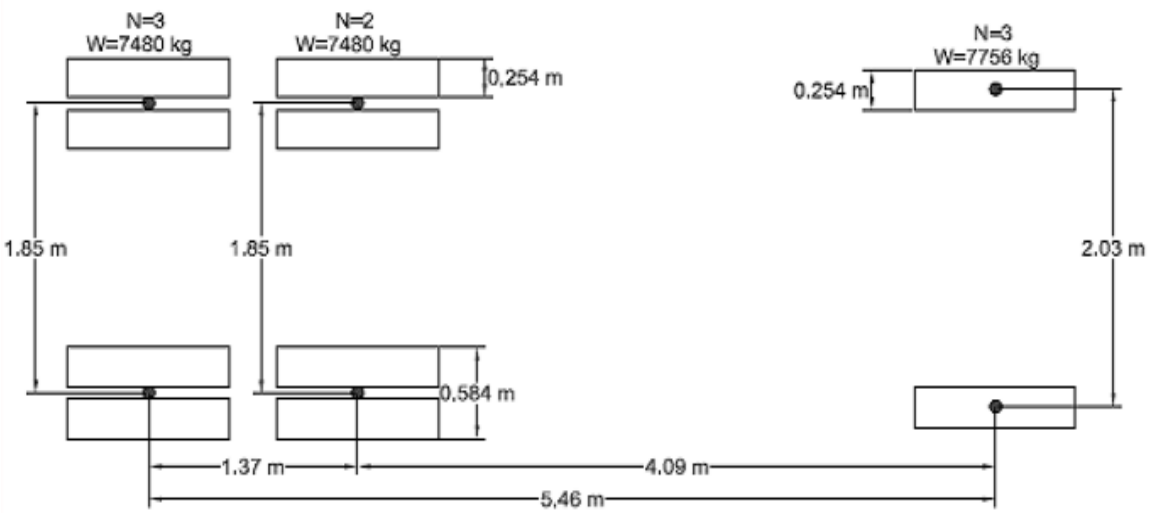

Fig. 14 Truck A footprint

rotation, the data acquisition system would receive a signal from the device and would subsequently mark the data. Using the data marks and the known circumference of the tire, the exact location of the truck could be determined as it traverses across the bridge.

For the high speed test, the autoclicker was removed but the truck was driven along load path 3. The autoclicker is shown in Fig. 20.

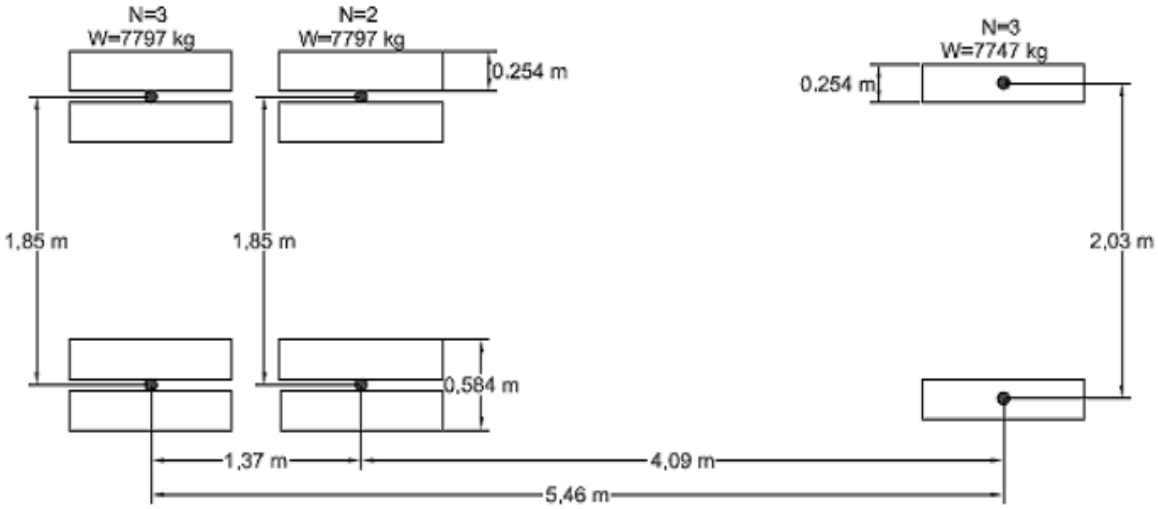

Fig. 15 Truck B footprint

Table 3 Load case descriptions

Load Case #	Load Case Description	Truck A Load Path	Truck B Load Path	Repetitions
1	Maximize Exterior Girder Response (Static)	1	1	3
2	Maximize First Interior Girder (psuedostatic)	1	2	2
3	Place One Truck in Each Travel Lane. Maximize Multiple Presence (psuedostatic)	3	4	3
4	Maximize Exterior Girder Response Truck B Following Truck A (psuedostatic)	1	1	2
5	Place On White Line of Right Travel Lane (psuedostatic)	5	-	2
6	High Speed	5	-	2

Table 4 Load path descriptions

Load Path #	Load Path Description	Load Path Horizontal Distance (m)	Load Combination Uses
1	East Most Location, 0.61 m off of parapet edge.	3.33	1, 2, 4, 5
2	Places Truck in East of Right Travel Lane	6.27	2
3	Center Truck In Right Travel Lane	6.58	3, 6
4	Center Truck in Left Travel Lane	10.64	3
5	Center Passenger Side Wheel on White Marking Line (over First Interior Girder) in Right Lane.	6.07	5

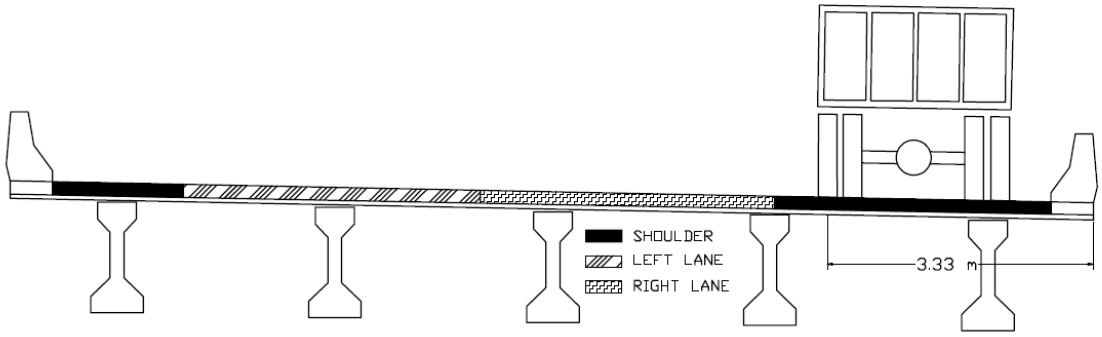

Fig. 16 Load Case 1, Truck A and Truck B backed toward each other, and Load Case 4, Truck B following Truck A

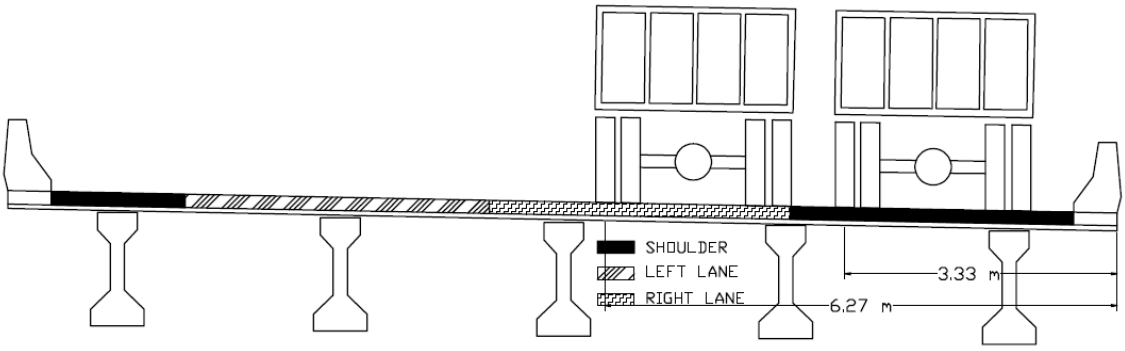

Fig. 17 Load case 2, Truck A (right) aside Truck B (left)

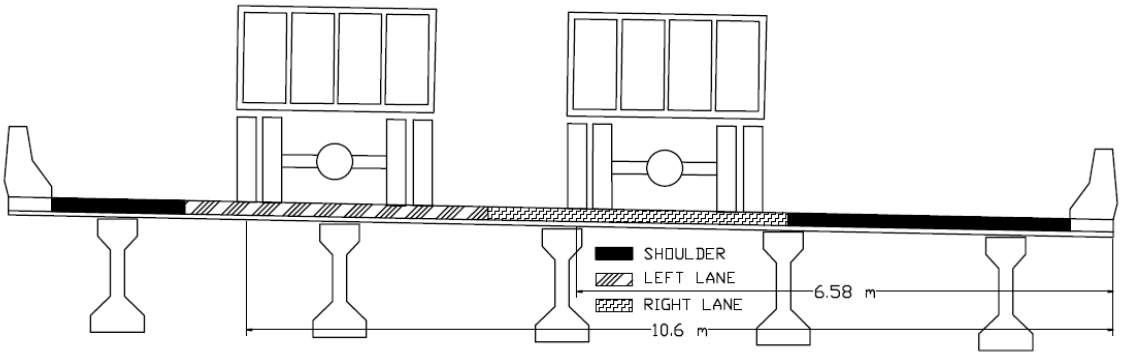

Fig. 18 Load case 3, Truck A (right) aside Truck B (left)

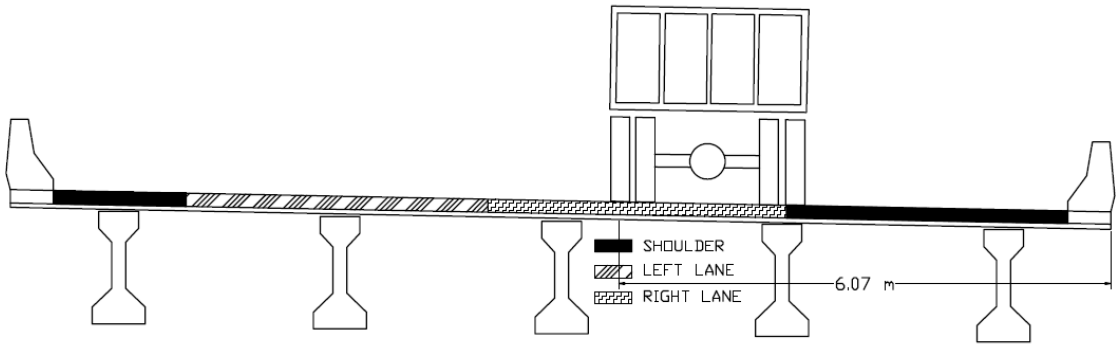

Fig. 19 Load Case 5, Truck A (psuedostatic), Load Case 6, Truck A (high speed)

4.3 Data Analysis

Before using the data collected from the live-load test, an analysis was required to determine whether or not the data was acceptable for use. Two analyses were conducted to ensure accurate data. First, multiple trials were run for each load case which allowed for a comparison between two sets of what should be identical data. All cases resulted in accurate data between the multiple runs for each load case. Fig. 21 provides an example of this comparison. The second analysis that was conducted on the live-load data was a strain vs. deflection analysis for each gauge in order to make sure all of the gauges were reading correctly. This analysis is effective because strain and deflection are inversely proportional. In order to make this comparison, the strain and the deflection (which was

multiplied by a negative multiplier) were plotted vs. all five girders for multiple positions. This analysis was completed on Load Case 4 which was found to provide an increasing shape with Girder 1 being the smallest and Girder 5 being the largest as determined by a hand calculation and modeling. Fig. 22 provides the results for a position of 24.4 m (80 ft) and Fig. 23 provides the results for a position of 18.3 m (60 ft). As shown by both figures, Girder 3 for deflection and Girder 5 for strain stray from the intended course of increasing. An argument could be made that the strains in Girders 3 and 4, as well as the deflection for Girders 4 and 5 were off though a quick hand calculation disproves this theory.

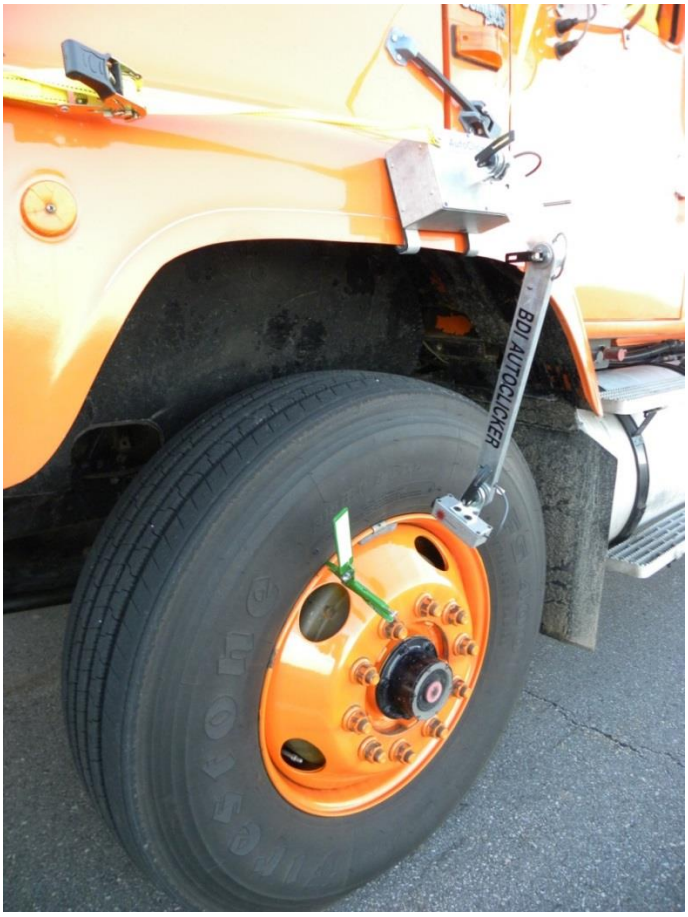

Fig. 20 Automated position tracking sensor, "Autoclicker," mounted on left front tire of Truck A

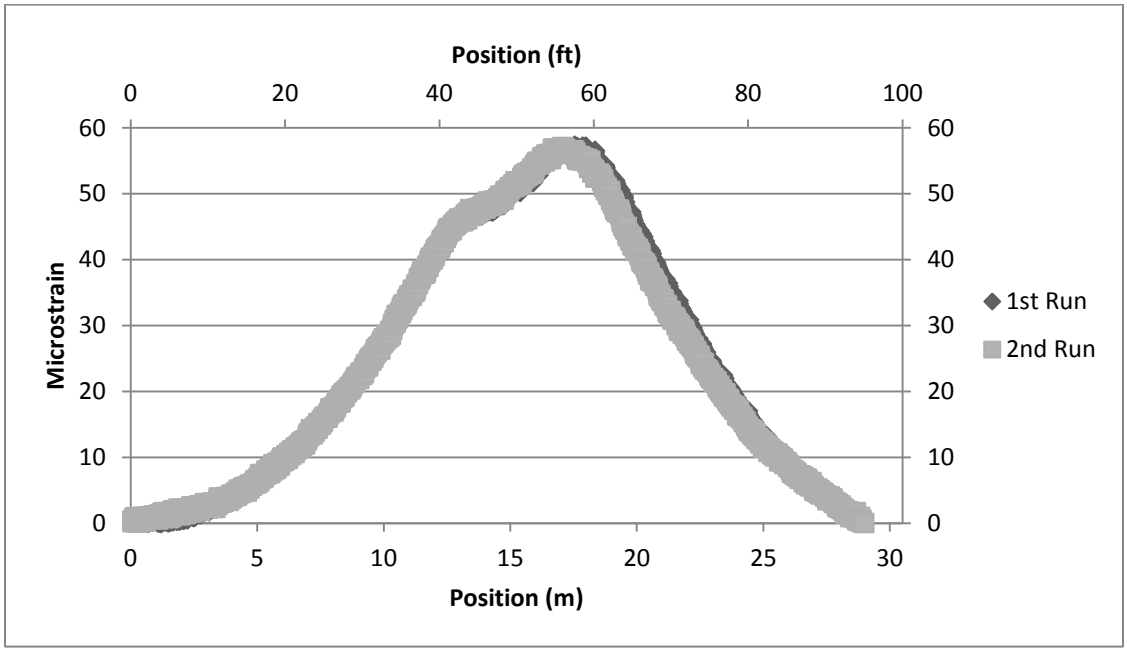

Fig. 21 Comparison of Load Case 3, 1st Run vs. 2nd Run

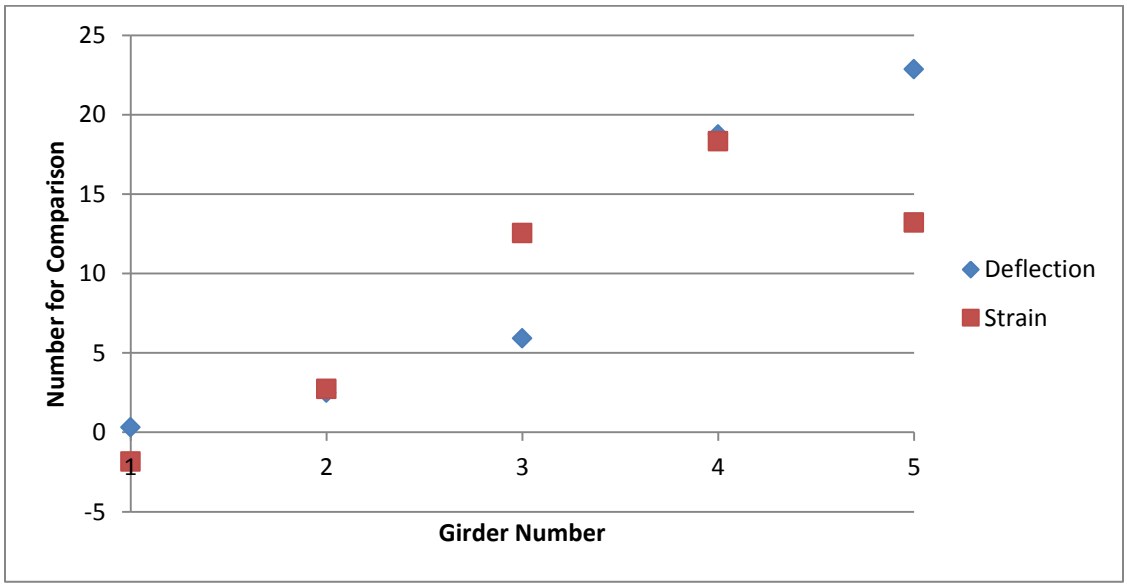

Fig. 22 Strain vs. Deflection comparison for Load Case 4 at 24.4 m

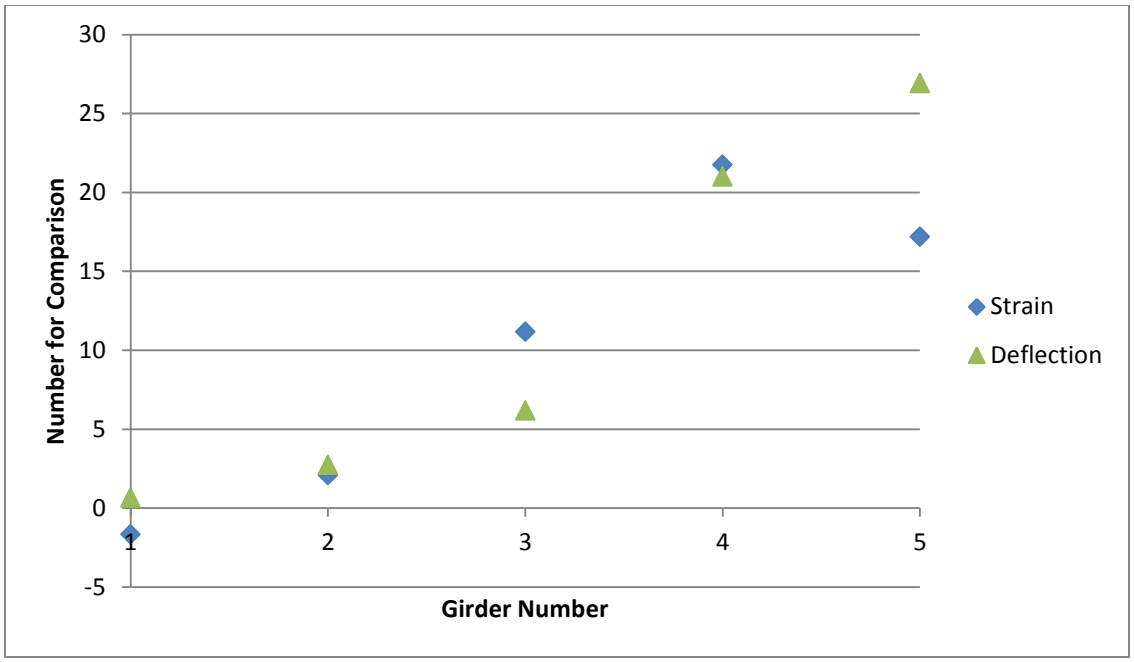

Fig. 23 Strain vs. Deflection comparison for Load Case 4 at 18.3 m

4.4 Static vs. Dynamic Comparison

Dynamic testing was conducted in order to determine the effect of a dynamic loading on the bridges strain and deflection. Dynamic testing was conducted by driving Truck A at both 7.2 m/s (16 mph) and 37.1 m/s following Load Path 5. This was deemed Load Case 6 and these dynamic effects were then compared to Load Case 5 which followed the same path, psuedostatically. Girder 4 was compared in both the strain and deflection cases to allow for consistency. The strain and deflection comparisons are shown in Fig. 24 and Fig. 25, respectively. The psuedostatic loading provides the largest maximums for both strain and deflection. In order to ensure this was correct, the order of maximum to minimum was compared for both strain and deflection. In both cases, the psuedostatic condition is the largest, followed by the fastest moving truck, followed by the medium moving truck. Because of this consistency and the fact that all three cases were measured by the same gauge within a short amount of time from each other, the

data looks to be correct. The reason this occurred is likely due to the fact that for the psuedostatic case, it was possible to guide the trucks exactly along the white line while for the high speed tests, the driver was unable to exactly line the right tires of the truck up with the right line. By being slightly off from the line, the strain and deflection in Girder 4 decreased causing the dynamic affects to be less than the psuedostatic effects. In addition, it was odd to not have a larger range from the dynamic tests; however, this is consistent with the gauges reading long-term data.

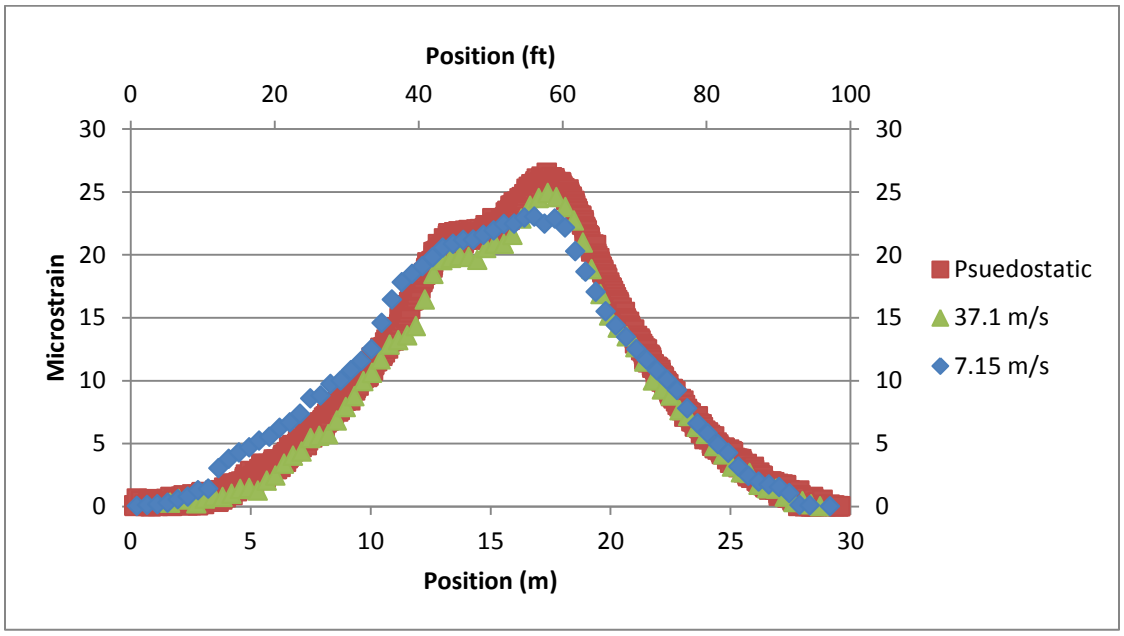

Fig. 24 Comparison of microstrain for psuedostatic and dynamic cases

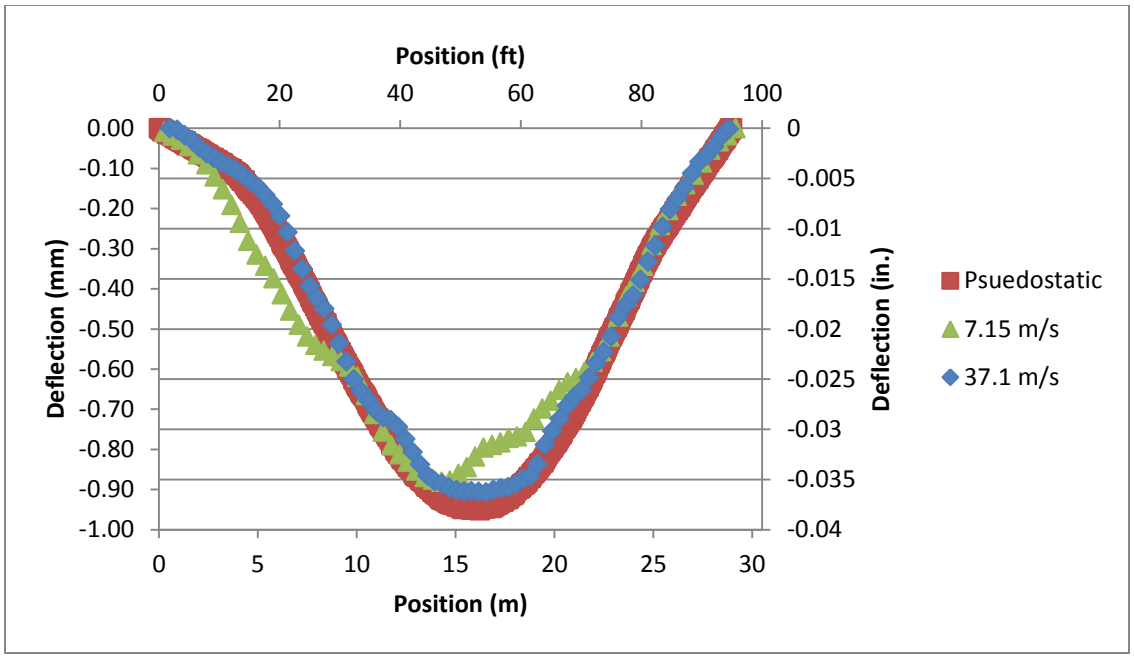

Fig. 25 Comparison of deflection for psuedostatic and dynamic cases

CHAPTER 5

FINITE-ELEMENT ANALYSIS

5.1 Description of FEM

The Utah Pilot Bridge finite-element model was created using SAP2000 v.15.0.0. All elements of the model were solids obtained by extruding poly areas to 305 mm (12 in.) thicknesses. The poly areas were mostly made up of four node rectangles, however, some four node trapezoids were utilized in the FEM.

In order for the model to function properly, the aspect ratio of the bridge was required to be at or below four, and not to exceed ten. For this FEM, the ratio between the longest and shortest dimension was kept at or below four in all occasions. Initially, the model was completed using larger poly areas, such as one for each entire cross section of the girder, however, when extruded and auto meshed, hundreds of solids were created pushing the limits on the aspect ratio criterion and causing the SAP2000 program to overload and crash. Limiting the poly areas to smaller rectangles and trapezoids allowed the program to function properly and provided aspect ratios under four.

The majority of the deck solids were 203mm x 203 mm x 305 mm (8”x8”x12”) rectangles with a maximum aspect ratio for the deck of two. The girder solids varied due to the shape and had aspect ratios between 1.5 and three. The barrier solid dimensions also varied due to shape but only had aspect ratios between 1.5 and 2. By limiting the poly areas to smaller dimensions, the extrusion process did not auto mesh and create unwanted solids. In addition, the smaller dimensions provide more accuracy in the model. Fig. 26 shows a cross-sectional view of the FEM solid elements.

The material properties in the deck, girders, and barriers were all altered in the

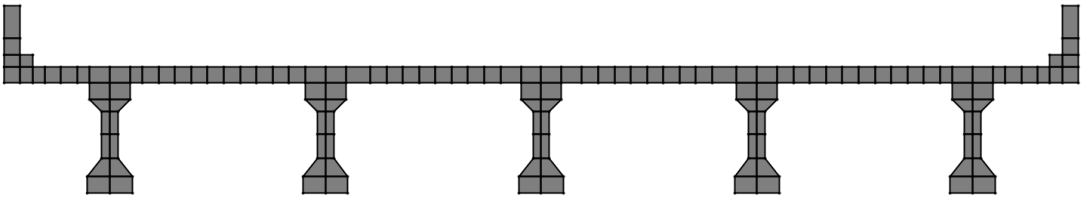

Fig. 26 FEM cross section

FEM to better represent the actual materials in the respective sections. The material properties, as well as the boundary conditions for the FEM, were adjusted until a strong correlation between the FEM and the actual bridge live-load data was achieved. The modulus of elasticity was kept within reason for each respective material. The final boundary conditions for the bridge were modeled as nearly fixed-fixed without restraints on all but the bottom of the middle girder as well as no restraints on the middle of the deck. This was caused by the stiffness created in the wing walls on the ends, as well as the fixed nature of the integral abutments.

Although the bridge has prestressing strands running through the concrete girders which would induce strain, the gauges attached to the bridge have been zeroed out so the effects of the strands would only be to stiffen the bridge. In order to determine the stiffening effect of the prestressing strands in the bridge, tendon elements were employed in the FEM. Tendons in an FEM are embedded elements that attach themselves to outer elements, such as solids. In this model, the tendons were modeled as loads, though the program allows the tendons to be modeled as elements which would include losses due to elastic shortening and time dependent effects. In addition, the program allowed a tendon to have up to six degrees of freedom; however, when encased in a solid element, the tendon element was restricted to only the three translational degrees of freedom because the three rotational degrees of freedom were restricted. Five tendons were used in total

for the FEM, one in each girder stretching from one abutment to the other. After testing the finite-element model, with and without the tendon elements, by checking the model with and without a truck load for each case, the tendon elements were found to have a negligible effect of less than one microstrain for the worst case scenario. Based on these tests, and the fact that the strain gauges on the bridge have been zeroed, tendons were neglected during FEM testing. In all, 19316 joints and 10752 solids were utilized in the FEM. Fig. 27 shows the 3D view of the FEM 3D.

5.2 Calibration

The calibration took place after the model was completed. The live-load test was used in order to conduct the calibration and a combination of end springs, boundary conditions, and material properties were changed in order to create a strong correlation between the live-load test and the FEM. Strains from the strain gauges and deflections from the deflectometers were compared to the strains and deflections of the model to

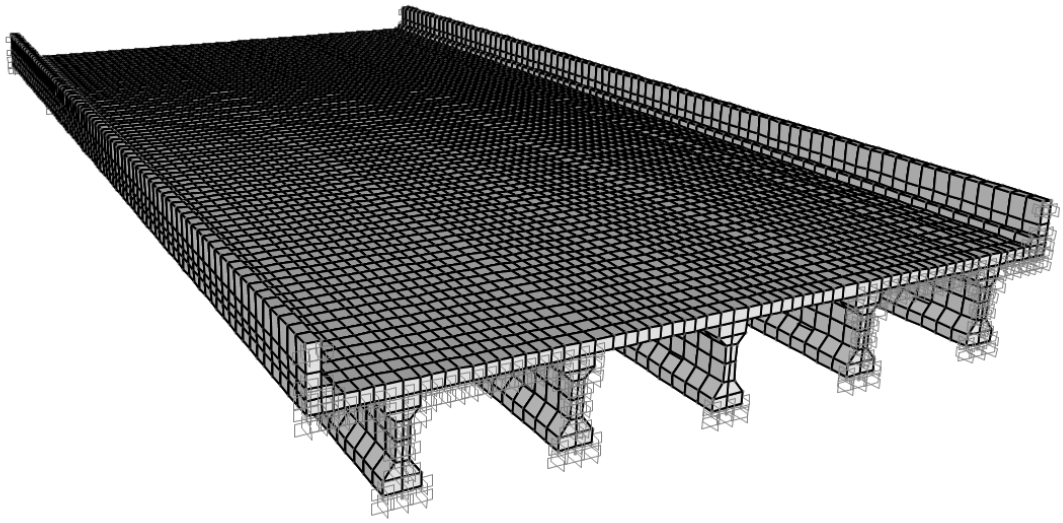

Fig. 27 FEM 3D view

determine the correlations. Nodes were placed on the FEM in the same respective location as the strain gauges and deflectometers on the actual bridge, which allowed the model to be more accurately calibrated.

The output data provided by the model gave deflections which allowed for a direct comparison between the live-load test data provided by the bridge sensors, and the FEM. The model however, did not provide strain as an output, but did provide the stress. From the stress, the strain could be calculated using Eq. 1. Because there are eight elements on the bottom of the girder near the node where the stress is being obtained, all eight element stresses were gathered and then averaged in order to obtain a more accurate reading for the FEM.

$$\sigma = E * \varepsilon$$

Eq. 1

where

σ = Stress

E = Young's Modulus of Elasticity

ε = Strain

Section BB of the bridge was used for calibration of strains due to the larger nature of the strains in the middle of the bridge as opposed to the strains gathered at Section DD, which had small strains being next to the abutment and were more likely to be affected by errors in the strain gauge. Upon checking the strain from the live-load test for each of the girders, Girder 5 behaved unexpectedly. After comparing the strain vs. deflection, it was made obvious that the data from Girder 5 could not be trusted and therefore it was not included in the comparison between the live-load test and the FEM.

Fig. 28- Fig. 30 show examples of these comparisons while Fig. 43 through Fig. 50 given in Appendix A provide more of the comparisons. Fig. 28 is a comparison between the live-load data and FEM for all five girders during Load Case 1 loading which gives a lateral distribution of the bridge. Fig. 29 is a comparison of the live-load data and FEM for only Girder 2 under the loading of Load Case 5. Fig. 30 provides a comparison between the live-load data and FEM microstrains which allows a means of seeing the correlation between the model and FEM. For this study, the R^2 value was over 0.95 suggesting a strong correlation between the two sets of data. Once a strong correlation was determined for strain, the calibration for deflection commenced.

For the calibration with respect to deflection, Section AA was used due to the section being at the midspan and having all five girders instrumented at this section. Like the strain gauge on Girder 5, the deflectometer on Girder 3 provided some questionable data. When comparing the strain vs. deflection of Girder 3, it was determined that the data provided by the deflectometer at Girder 3 could not be used and was discarded. Fig. 31 – Fig. 33 show examples of the comparisons between the live-load data and the FEM data for deflection. Fig. 31 compares the live-load data and FEM for all five girders during Load Case 4 loading, providing insight into the lateral distribution of the bridge. Fig. 32 is a comparison of the live-load data and FEM for only Girder 5 under the loading of Load Case 5. Fig. 33 shows the comparison of the microstrain for the live-load data and FEM and provides an R^2 value of 0.99 suggesting a strong correlation between the two sets of data. Because both strain and deflection are strongly correlated, the model could be used to compare the actual bridge to the AASHTO LRFD Bridge Design Specifications.

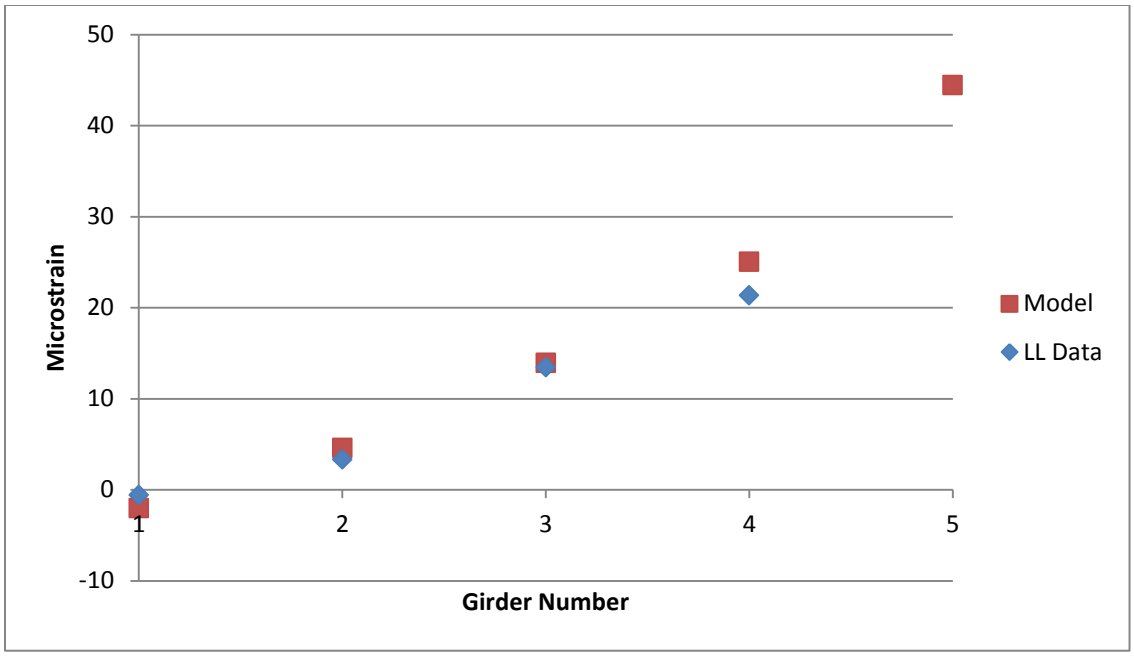

Fig. 28 Microstrain comparison near midspan between live-load data and model for Load Case 1, all girders

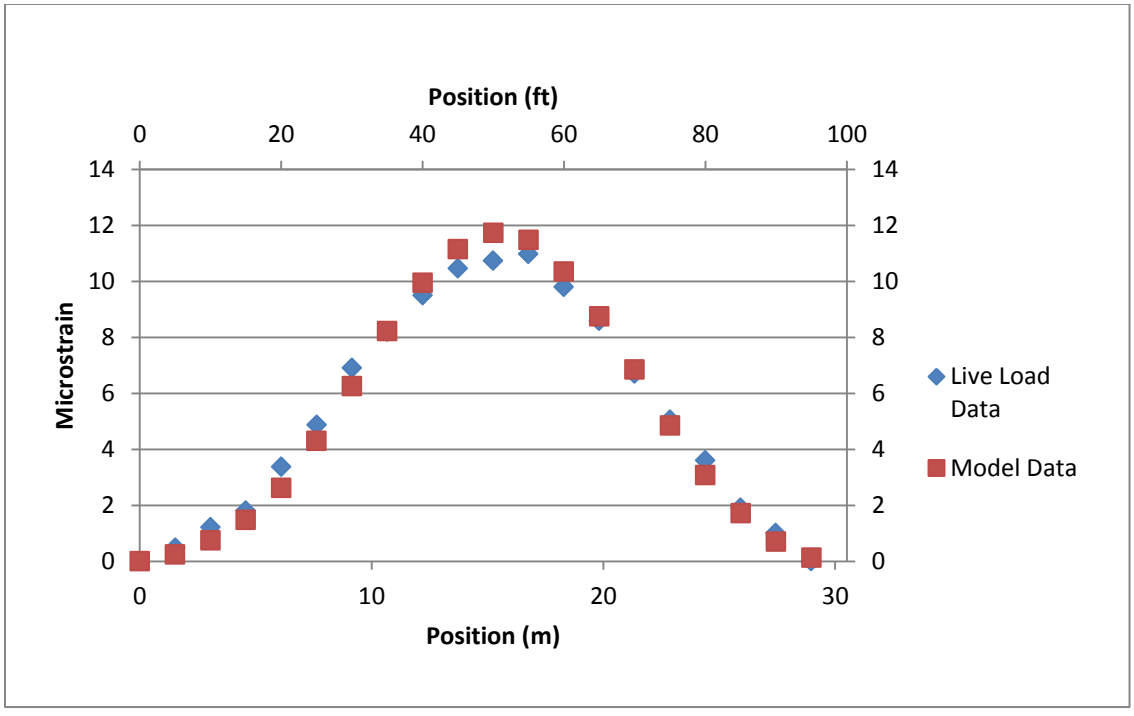

Fig. 29 Microstrain comparison near midspan between live-load data and model for Load Case 5, Girder 2

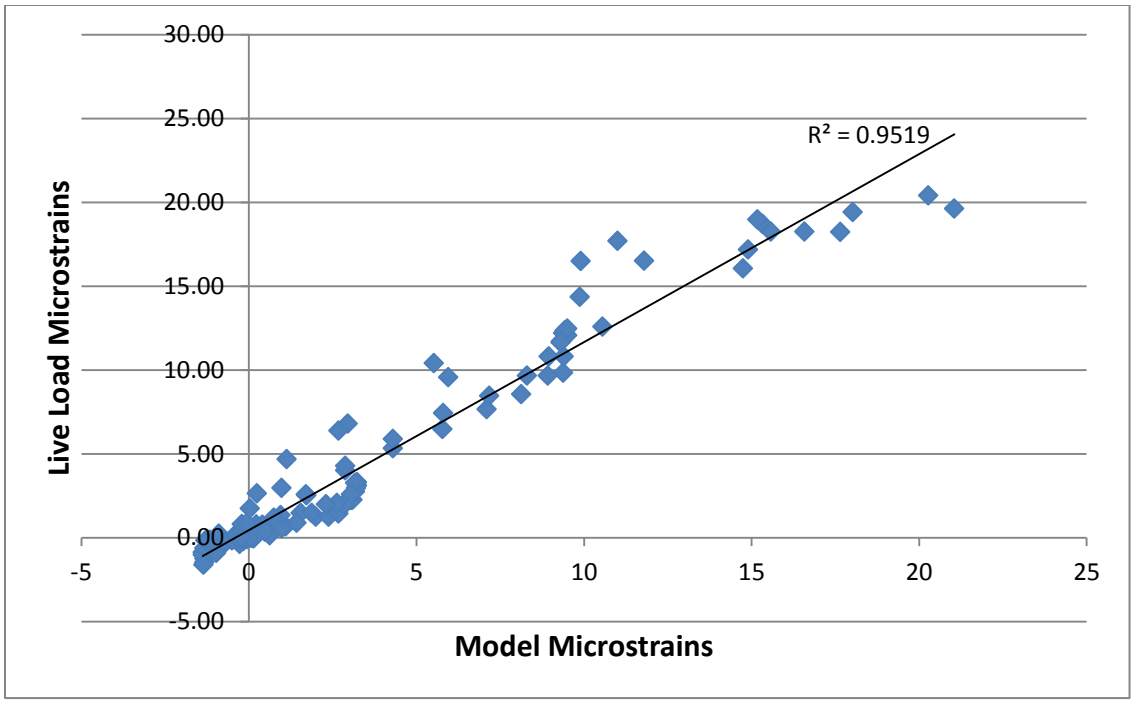

Fig. 30 Live-load microstrain vs. model microstrain near midspan for all girders

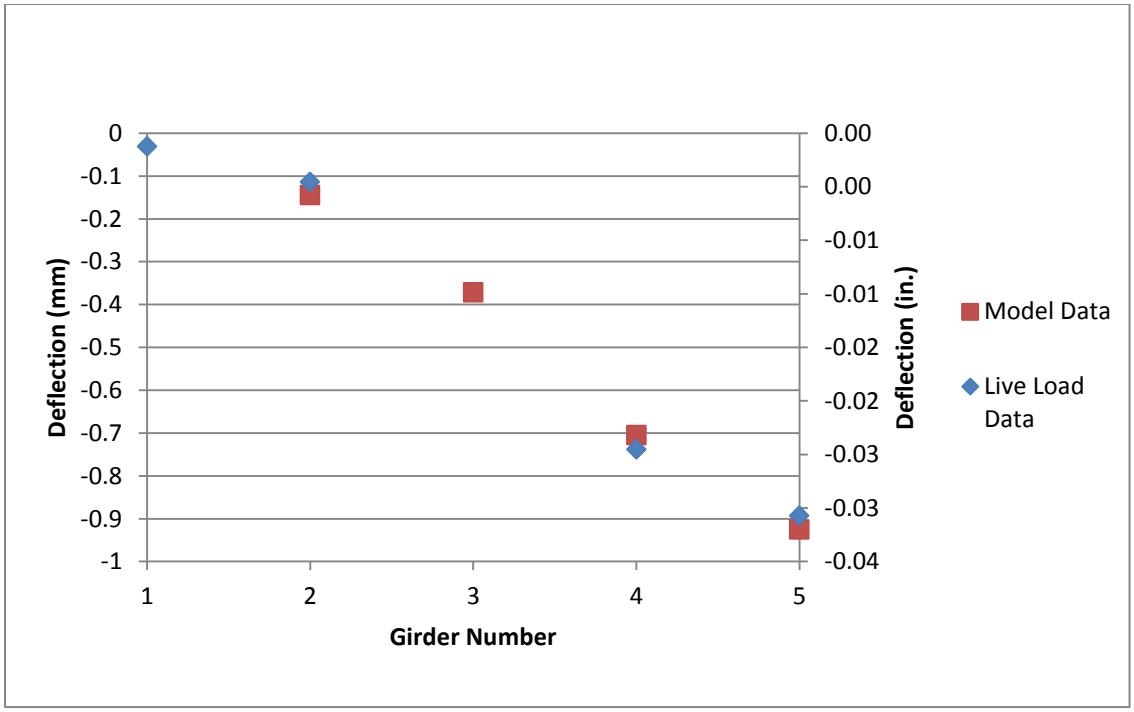

Fig. 31 Deflection comparison at midspan between live-load data and model for Load Case 1, all girders

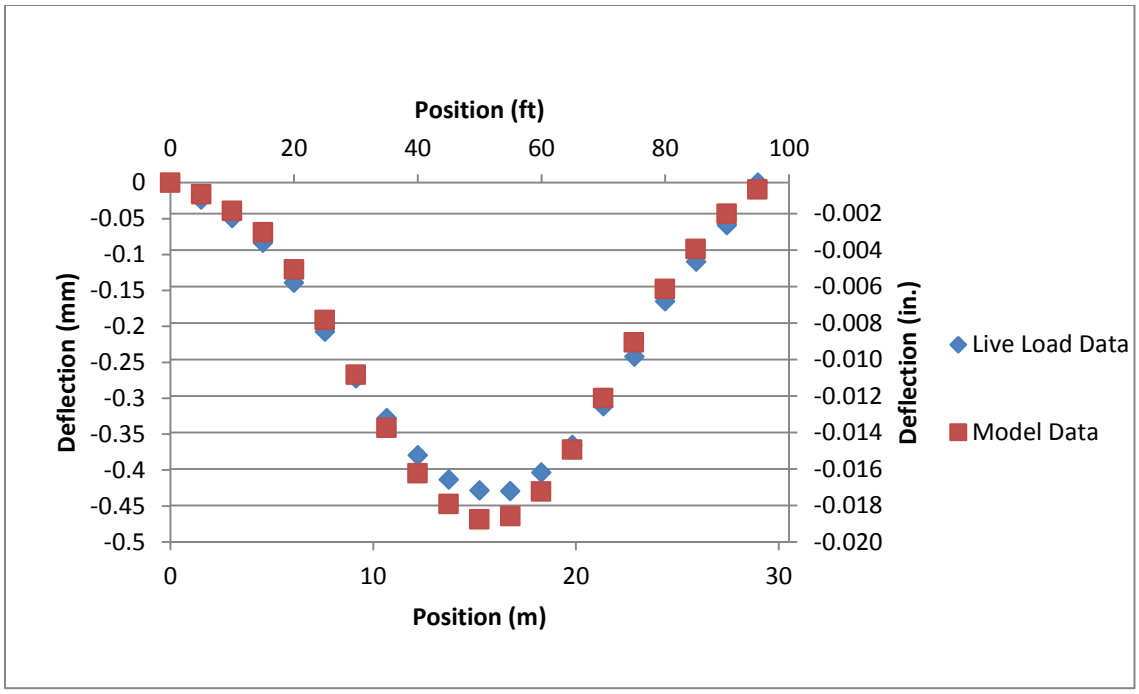

Fig. 32 Deflection comparison at midspan between live-load data and model for Load Case 5, Girder 5

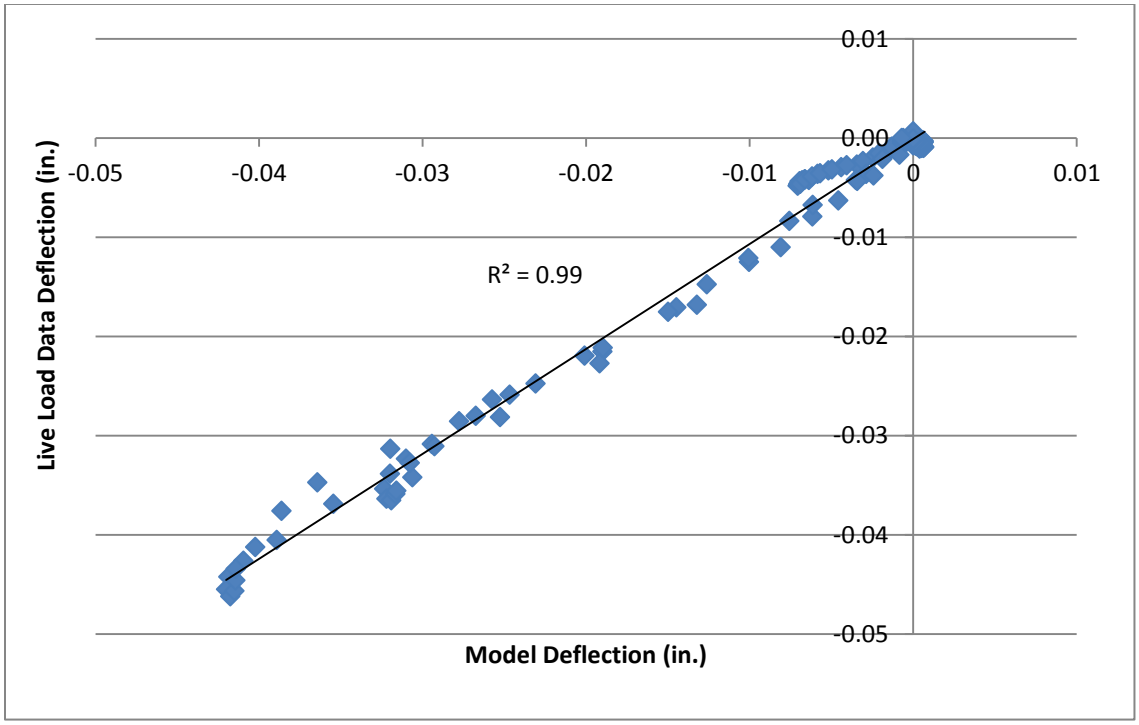

Fig. 33 Live-load deflection vs. model deflection at midspan for all girders

5.3 Distribution Factors

A live-load distribution factor determines how well a load will be distributed laterally across the girders of a bridge. Either shear or moment can control when using distribution factors however, for this study, only moment distribution factors were considered because they could be measured in the field. The live-load distribution factors obtained through the FEM were compared to those calculated using the Fifth Edition of AASHTO LRFD Bridge Design Specifications (AASHTO, 2010). The equations provided by the code include factors for exterior girders, different skews, different lengths, and many different bridge characteristics. All bridges designed by the AASHTO code, however, do not take into effect the different types of abutments available for bridge construction. The code rather assumes that every bridge is simply supported. This results in bridges being overly conservative and by doing studies on each of the different bridge abutment types, for different types of girders, bridges could be constructed more economically with more reasonable factors of safety.

5.3.1 Finite-Element Model Distribution Factors

To obtain the correct maximum moments for the FEM in order to determine the distribution factors, the FEM was loaded with an AASHTO HS20-44 truck. This truck has a loading of 35.6 kN (8 kips) on the front axle and a loading of 142 kN (32 kips) on the middle and back axles. The front and middle axles have a distance of 4.27 m (14ft) and the middle and back axles have a distance between 4.27 m (14 ft) and 9.14 m (30 ft). After a quick calculation, it was determined that the distance of 4.27 m (14 ft) between the middle and back axles would control. The transverse distance between the wheel spacing for all axles is 1.83 m (6 ft).

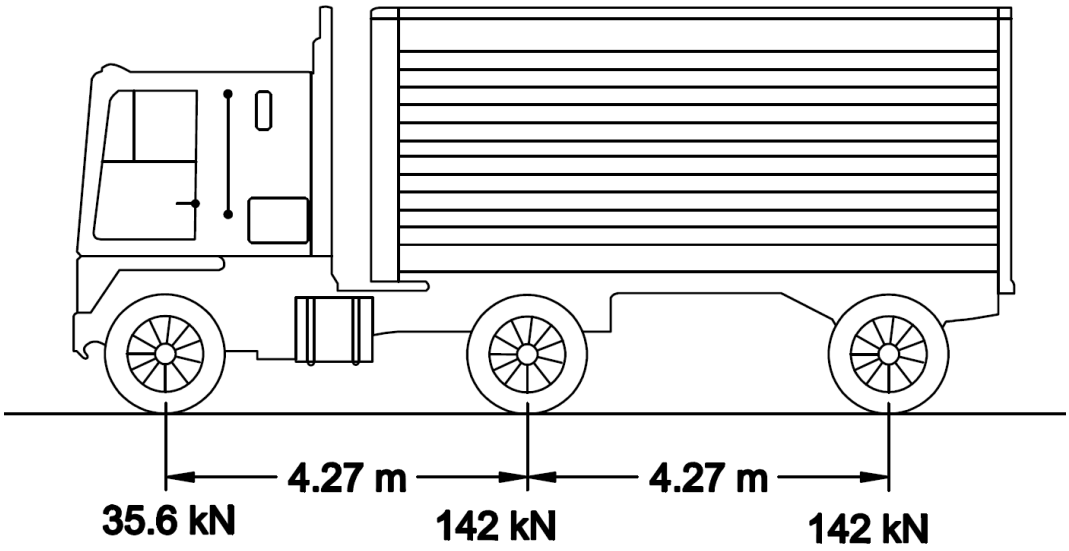

Fig. 34 AASHTO HS20-44 Truck

In order to maximize the moment, based on the position of the truck on the bridge in the longitudinal direction, a resultant force analysis was conducted and the middle axle of the truck was determined to need to be placed 0.71 m (2.33 ft) off the center of the bridge towards the north. In order to maximize the moment the interior and exterior girders might see under both single and double lane loadings in the transverse direction, nine different load cases were run and all five girder moments were checked for each case. The maximum single and multiple lane moments were obtained for both the interior and exterior girders. In order to determine the distribution factor, the 2D simply supported moment was calculated, placing the truck at the same longitudinal location as was seen on the model. The distribution factors for the FEM could then be calculated using Eq. 2 for single lanes and Eq. 3 for multiple lanes. After acquiring these distribution factors, the results seemed abnormally conservative. In order to ensure these numbers were reasonable, the distribution factors were also obtained using a fixed-fixed moment. This is not how the code obtains the distribution factor, regardless of fixity, but

this would enable us to more easily compare to the codes distribution factors. These equations are provided in Eq. 4 and Eq. 5.

$$DF^1 = \frac{1.2 * M_{FEM}}{M_{SS}}$$

Eq. 2

$$DF^2 = \frac{M_{FEM}}{M_{SS}}$$

Eq. 3

$$DF^1 = \frac{1.2 * M_{FEM}}{M_{FF}}$$

Eq. 4

$$DF^2 = \frac{M_{FEM}}{M_{FF}}$$

Eq. 5

where

DF^1 = Distribution factor for single lane loads

DF^2 = Distribution factor for multiple lane loads

M_{FEM} = Moment of the finite-element model

M_{SS} = Moment of a simply supported beam with the same loading

M_{FF} = Moment of a fixed-fixed beam with the same loading

5.3.2 AASHTO Distribution Factors

The AASHTO LRFD Bridge Design Specifications designate the Perry Bridge to be type "k" in Table 4.6.2.2.1-1. The distribution factors for interior girders one lane and multiple lanes were therefore obtained using Eq. 6 and Eq. 7. For exterior girders with two or more design lanes loaded, the distribution factors were acquired by using a factor multiplied by distribution factor for the interior girders shown in Eq. 8.

$$DF_I^1 = 0.06 + (\frac{S}{14})^{0.4}(\frac{S}{L})^{0.3}(\frac{K_g}{12.0Lt_s^3})^{0.1}$$

Eq. 6

$$DF_I^2 = 0.075 + (\frac{S}{9.5})^{0.6}(\frac{S}{L})^{0.2}(\frac{K_g}{12.0Lt_s^3})^{0.1}$$

Eq. 7

$$K_g = n(I + Ae_g^2)$$
$$n = \frac{E_B}{E_D}$$

$$DF_E^2 = e * DF_I$$

Eq. 8

$$e = 0.77 + \frac{d_e}{9.1}$$

where

DF_I^1 = Distribution factor for the single lane loaded interior girder

DF_I^2 = Distribution factor for the multiple lane loaded interior girder

DF_E^2 = Distribution factor for the multiple lane loaded exterior girder

S = Girder spacing (ft)

L = Span length of beam (ft)

K_g = Longitudinal stiffness parameter

t_s = Depth of concrete slab (in.)

E_B = Modulus of elasticity of beam material (ksi)

E_D = Modulus of elasticity of deck material (ksi)

I = Moment of inertia of beam (in.^{4})

A = Area of cross-section (in.^{2})

e_g = Distance between the centers of gravity of the basic beam and deck (in.)

e = Correction factor

d_e = Overhang distance (ft)

For exterior girders with only one design lane loaded, the lever rule was required to determine the distribution factor. In order to show the lever rule, Fig. 35 provides the variables needed. First, the R_A term is found by taking a moment about point B and setting it equal to zero, as shown in Eq. 9.

$$R_A = \frac{P(S + d_e - 5)}{S}$$

Eq. 9

where

S = Girder spacing (ft)

d_e = Overhang distance (ft)

P = Truck load

R_A = Reaction of exterior girder

In order to determine the fraction of truck weight, P, that is carried by the exterior girder we remove the P term. The multiple presence factor for a single lane loaded case is 1.2 and therefore, the moment distribution factor for the exterior girder single lane loaded case is given in Eq. 10.

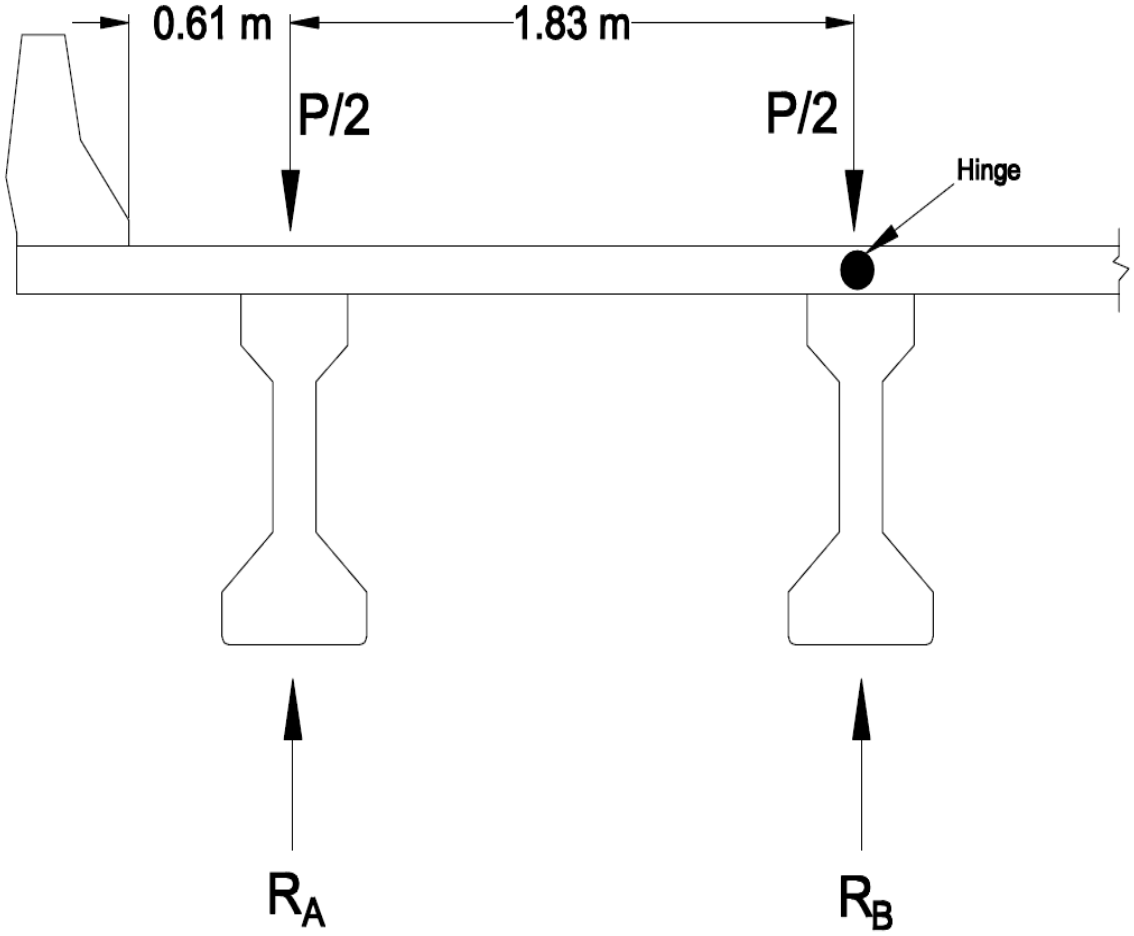

Fig. 35 Lever Rule variables

$$DF_E^1 = \frac{1.2 \times (S + d_e - 5)}{S}$$

Eq. 10

where

DF_E^1 = Distribution factor for the single lane loaded exterior girder

5.3.3 AASHTO Equation Range of Applicability

Table 5 provides criteria that must be met in order to use the AASHTO LRFD Specification distribution factor equations.

5.3.4 Resulting Distribution Factors

Once all of the distribution factors had been calculated for the AASHTO LRFD Specifications, and the FEM, the percent difference was calculated in order to determine how well our current codes predict the actual nature of a concrete girder bridge with integral abutments. In all cases using the simply supported 2D beam, the code was overly conservative for the design of these type of bridges. The maximum percent

Table 5 Ranges wherein the AASHTO equations are valid

Range of Applicability
$3.5 \leq S \leq 16$
$4.5 \leq t_s \leq 12$
$20 \leq L \leq 240$
$4 \leq N_b$
$10{,}000 \leq K_g \leq 7{,}000{,}000$
$1.0 \leq d_e \leq 5.5$

difference was 78% conservative for one lane, interior girders while the governing case was the exterior girder, two lane case which was 55% conservative. All girder cases are given in Table 6. The reason for these highly conservative distribution factors is because the code assumes the bridge to be simply supported while in all actuality, an integral abutment bridge has partial fixity in its ends. While it is better to be over-conservative as opposed to being non-conservative, if an integral abutment factor could be determined for each different type of bridge girder, the design of integral abutment bridges could be made more economical. If complete fixity were taken into account in this case by providing a distribution factor obtained using a fixed-fixed moment, a more realistic moment is provided and the results become less conservative. The results in Table 6 show that the maximum percent difference between the FEM and fixed-fixed distribution factors was only 47% conservative, though the exterior with two lanes loaded was non-conservative by 8%. This was likely due to the bridge not having complete fixity but still having partial fixity. In order to determine how much fixity was in the bridge, the FEM was optimized by taking the controlling case and setting the percent difference to zero by altering the moment. Upon determining the moment, the approximate percent fixity was determined, using linear interpolation and the one non-conservative case, to be 94%.

5.4 Parametric Study

In order to see the different effects specific variables have on the distribution factors, a parametric study was conducted. Looking at the variables that are restricted in the AASHTO LRFD Bridge Design Specifications and then adding fixity; span length, deck thickness, edge distance, skew, and fixity were chosen as the different variables to do parametric studies on. In order to conduct these studies, new models were created for

Table 6 Distribution factors for all girder cases

Girder Case	AASHTO LRFD (1)	SS FEM (2)	% Difference =(1-2)/(1)	Fixed FEM (3)	% Difference =(1-3)/(1)	Optimized FEM (4)	% Difference =(1-4)/(1)
One Lane							
Interior	0.54	0.12	78%	0.28	47%	0.26	51%
Exterior	0.87	0.31	64%	0.74	15%	0.68	22%
Two Lanes							
Interior	0.76	0.19	75%	0.46	39%	0.43	44%
Exterior	0.80	0.36	55%	0.86	-8%	0.80	0%

every case and then loaded with the AASHTO HS20-44 truck at the same position of maximum moment that was determined in the Distribution Factor section, with the middle axle of the truck being placed 0.71 m (2.33 ft) off center of the bridge towards the north. Except for the parametric study dealing with fixity, each of the models were simply supported to ensure as controlled of a test as possible.

For each of the parametric models, the bridge was configured with the same general components as the original FEM. After testing, the distribution factors of each model was obtained in the same way that the original FEM's distribution factors were obtained, and then compared to the distribution factors obtained from the AASHTO LRFD Specifications, taking into account the altered variables. Due to the initial conditions being selected and calibrated based on the Perry Bridge, the general trend of the distribution factors will provide more insight into how the variables affect the bridge, as opposed to a comparison of the magnitudes. Therefore, in each case, a distribution factor ratio will be provided and plotted against the parameter in question. The ratio will be the FEM distribution factor divided by the AASHTO distribution factor which means that a value recorded below one will reveal that the AASHTO LRFD Specifications are

conservative while a value recorded above one will show that the AASHTO LRFD Specifications are non-conservative as compared to the FEM. Fig. 51 through Fig. 63 in Appendix B provide all of the comparison figures not included in this section.

5.4.1 Span Length

The first variable selected was the span length of the bridge. The range tested was at intervals of 9.1 m (30 ft), beginning at 15.2 m (50 ft) and ending at 51.8 m (170 ft). These lengths were chosen to encompass most of the lengths allowed by the equations given in the AASHTO LRFD Specifications. After obtaining the distribution factors, the controlling percent differences determined the AASHTO LRFD Specifications to be between 18% and 30% conservative. Fig. 36 provides the ratio of distribution factors between the FEM and AASHTO LRFD Specifications vs. the length of span for the governing case of exterior girders with one lane loaded. This was the only case that when the span length increased, the amount of conservatism increased. This is due to the one lane loaded, exterior girder being determined by the lever rule which doesn't take span length, fixity, or deck thickness but only acknowledges edge distance, skew, and spacing. The exterior girder, two lane loaded case is also provided because it is relatively close to the controlling distribution factor and if the lever rule were fixed, this case would govern. The exterior girder, two lane loaded case determined the AASHTO LRFD Specifications to be between 24% non-conservative and 8% conservative. The 15.2 m (50 ft) FEM distribution factor starts conservative but as the span length is increased, the AASHTO LRFD Specifications become immediately non-conservative and continue to become more and more non-conservative. Fig. 37 provides the ratio of distribution factors between the FEM and AASHTO LRFD Specifications vs. the length of span for

the case of exterior girders with two lanes loaded. It seems odd that the code would allow for non-conservatism; however, multiple studies have also seen this case be conservative in their studies (Dicleli and Erhan 2009, Hodson et al. 2012).

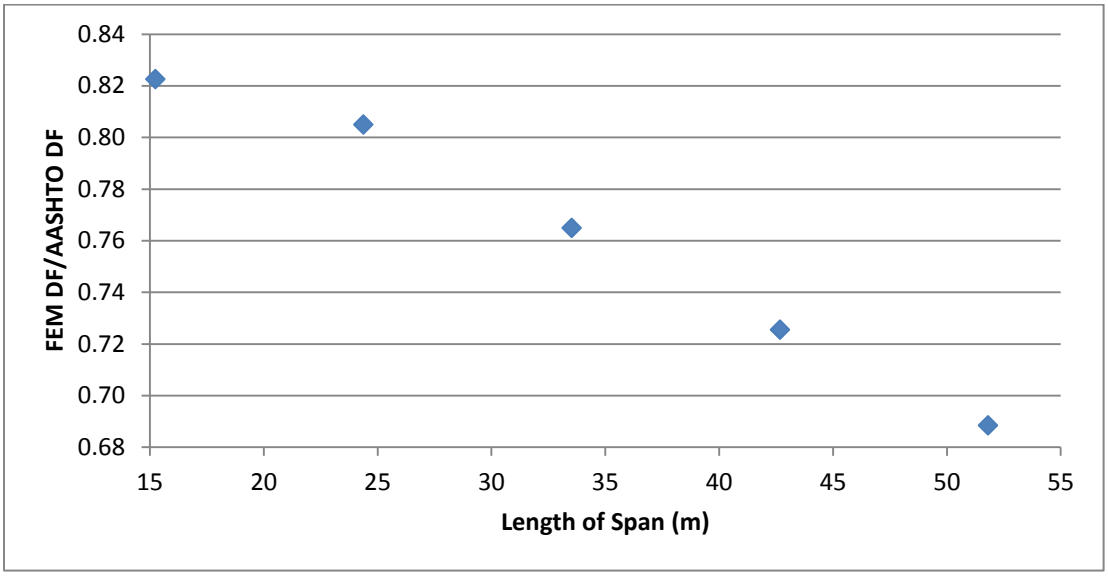

Fig. 36 FEM Distribution Factor/AASHTO Distribution Factor vs. length of span for the case with exterior girder, one lane loaded

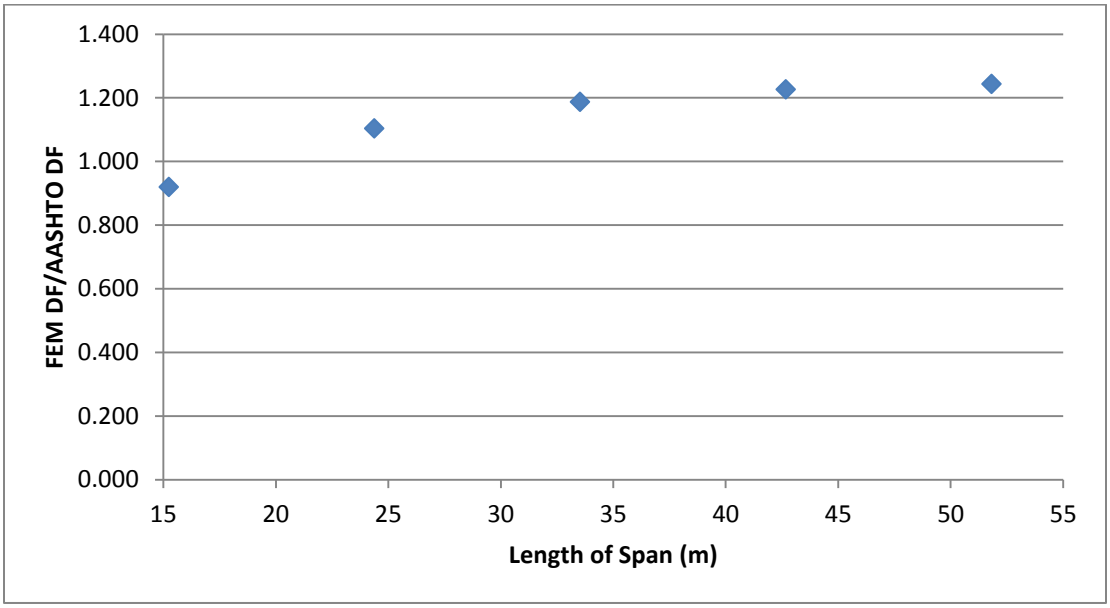

Fig. 37 FEM Distribution Factor/AASHTO Distribution Factor vs. length of span for the case with exterior girder, two lanes loaded

5.4.2 Fixity

The next parametric study was conducted on the fixity of the bridge. The first bridge tested was a simply supported bridge and then springs were slowly added and then increased until a completely fixed-fixed bridge was tested. The tests included 1- simply supported, 2- transverse springs with stiffnesses of 12.2 kN/m (10 k/in.), 3- transverse springs with stiffnesses of 122 kN/m (100 k/in.), 4- transverse springs with stiffnesses of 1216 kN/m (1000 k/in.), 5- the FEM based on the real bridge, and 6- fixed-fixed. After obtaining the distribution factors, the controlling percent differences determined the AASHTO LRFD Specifications to be between 20% and 65% conservative. Fig. 38 provides the ratio of distribution factors vs. the fixity of the bridge for the governing case of exterior girders with a one lane loaded.

As the fixity of the bridge increases, the AASHTO LRFD Specifications become more and more conservative. This again is likely due to the lever rule not taking into account fixity; however, none of the AASHTO equations take into account fixity. Therefore, all of the cases for the AASHTO LRFD Specification distribution factors also became more and more conservative. Still, the two lane loaded, exterior girder case for the AASHTO LRFD Specification distribution factors had a point of being non-conservative ranging from between 10% non-conservative, and 56% conservative. Due to being non-conservative, the distribution factors for this case should be altered in the AASHTO LRFD Specifications. Fig. 39 provides the ratio of distribution factors vs. the fixity of the bridge for the case of exterior girders with two lanes loaded. Incorporating fixity into the AASHTO LRFD Specification equations is a recommendation of this study.

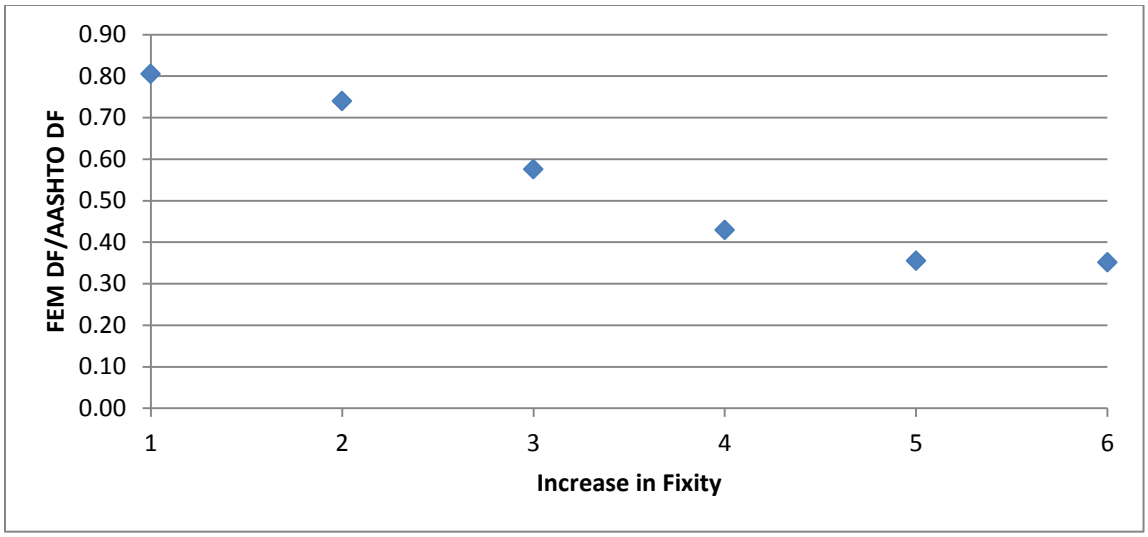

Fig. 38 FEM Distribution Factor/AASHTO Distribution Factor vs. fixity for the case with exterior girder, one lane loaded

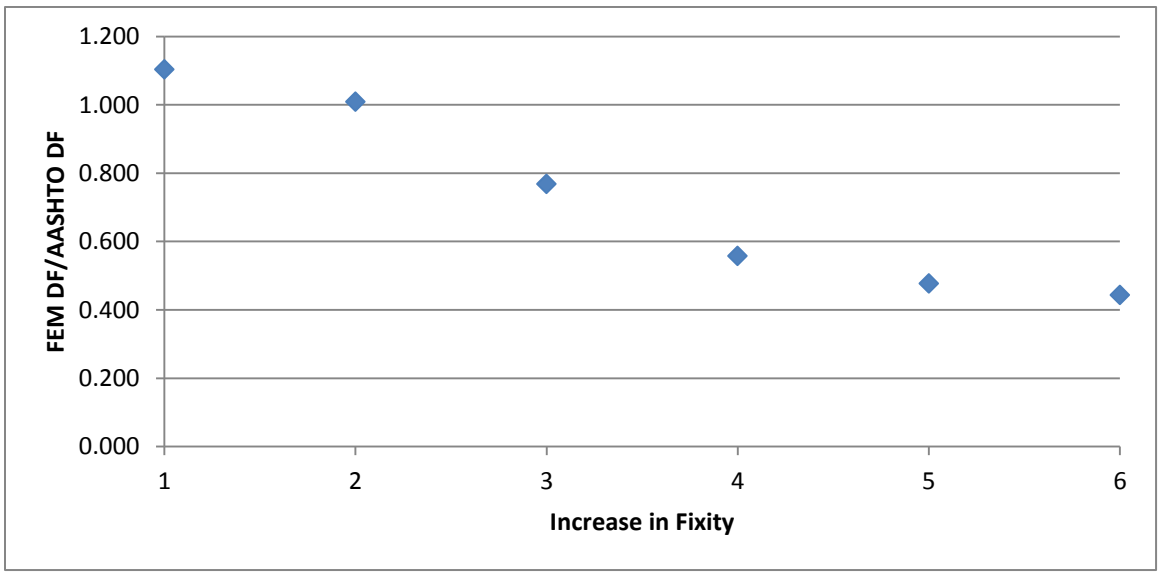

Fig. 39 FEM Distribution Factor/AASHTO Distribution Factor vs. fixity for the case with exterior girder, two lanes loaded

5.4.3 Deck Thickness

The next variable tested was the deck thickness. Distribution factors for thicknesses of 0.15 m (6 in.), 0.20 m (8 in.), 0.25 m (10 in.), and 0.30 m (12 in.) were all determined. After obtaining the distribution factors, the controlling percent differences

again came from the exterior single loaded case and determined the AASHTO LRFD Specifications to be between 18% and 23% conservative. The exterior girder, two lane loaded case determined the AASHTO LRFD Specifications to be between 4% and 19% non-conservative. As opposed to providing figures for both cases, only the exterior girder, two lane loaded case will be provided throughout the rest of the paper because the lever rule has already been proven to be too conservative, while the more important fix would be to prevent being non-conservative in the code. Fig. 40 provides the ratio of distribution factors vs. deck thickness for the case of exterior girders with a two lanes loaded. As the deck thickness increases, the AASHTO LRFD Specifications become more and more non-conservative. Like the increase in span length, all cases become more non-conservative, except for the exterior girder single lane loaded case. This is also due to the lack of the lever rule taking into account the deck thickness.

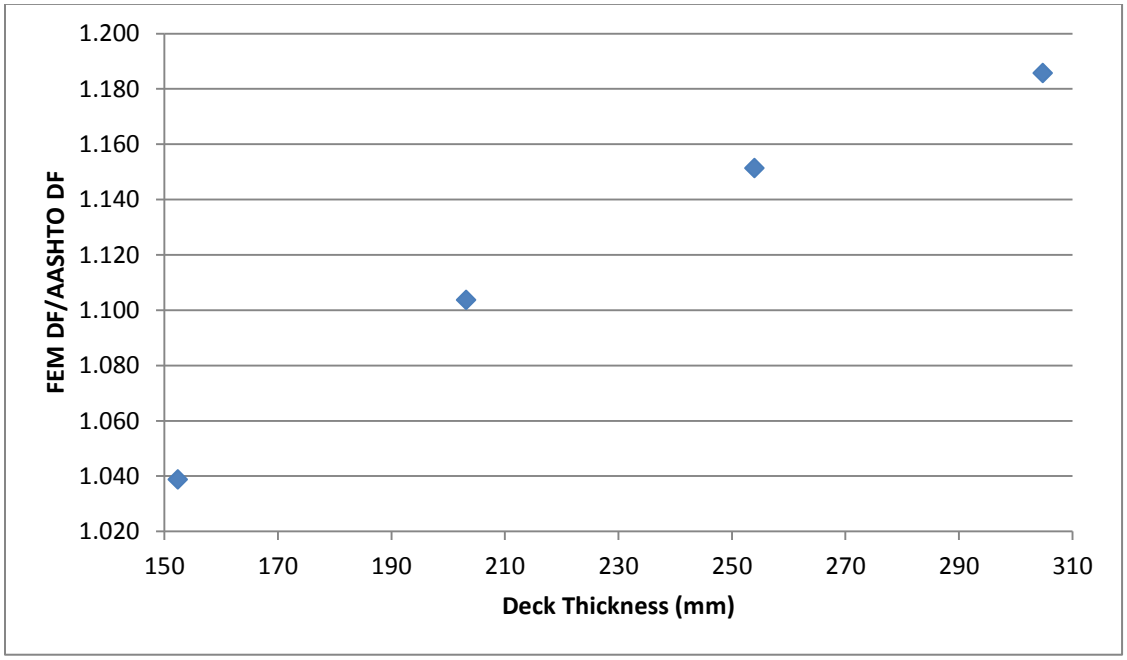

Fig. 40 FEM Distribution Factor/AASHTO Distribution Factor vs. deck thickness for the case with exterior girder, two lanes loaded

5.4.4 Skew

Different skews for the bridges were compared for the next parametric study. Skews every 15 degrees from 0 to 60 were compared. After obtaining the distribution factors, the controlling percent differences determined the AASHTO LRFD Specifications to be between 20% and 65% conservative for the single loaded exterior girder. The two lane loaded exterior girder determined the AASHTO LRFD Specifications to be between 10% non-conservative and 56% conservative. Fig. 41 provides the ratio of distribution factors vs. bridge skew for the governing case of exterior girders with a two lanes loaded. As the skew angle increases, the AASHTO LRFD Specifications become more conservative except for between 45 degrees and 60 degrees in which the Specifications become less conservative. This trend occurs for all load cases because the skew affects the lever rule, the AASHTO LRFD Specification equations, as well as the FEM.

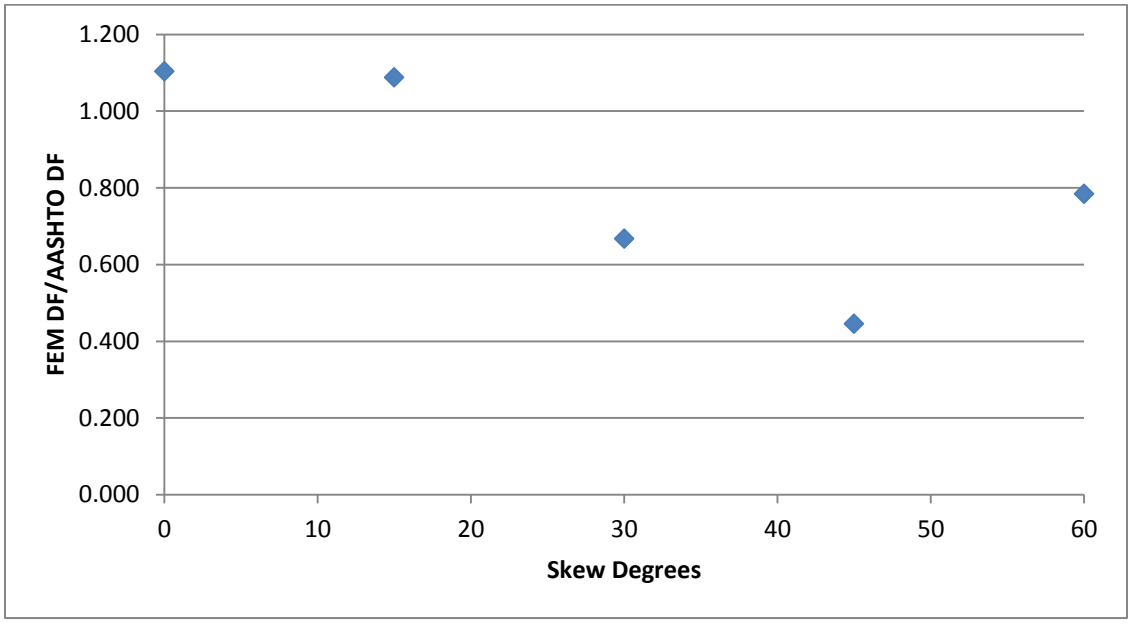

Fig. 41 FEM Distribution Factor/AASHTO Distribution Factor vs. skew degrees for the case with exterior girder, two lanes loaded

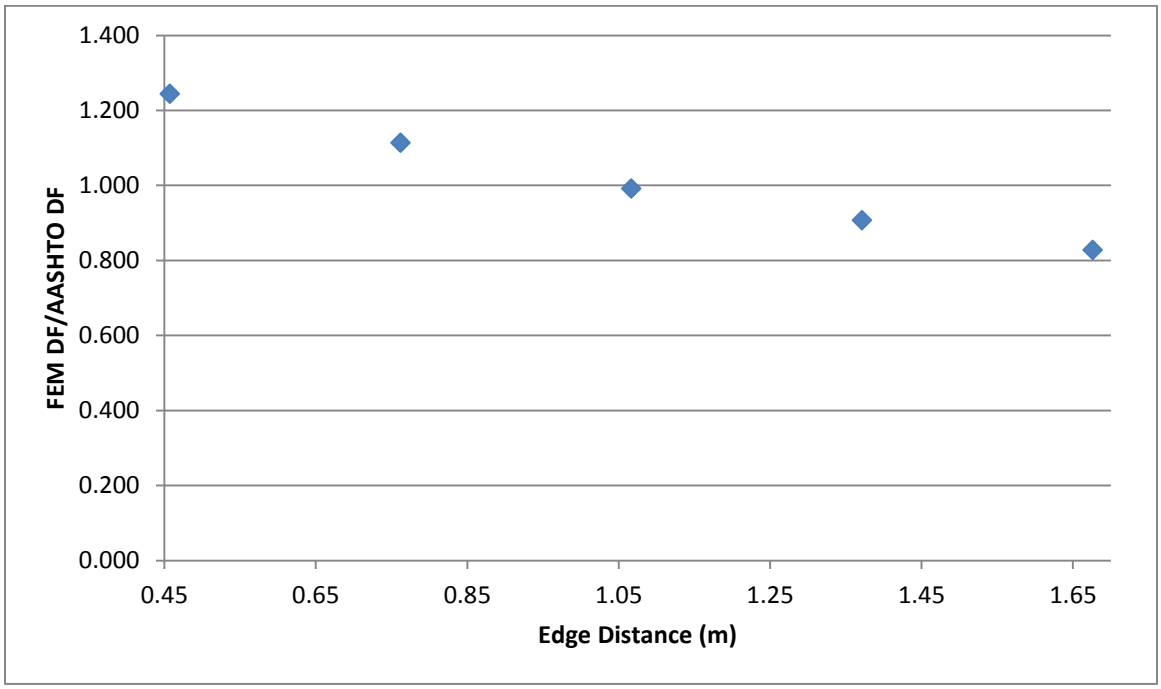

Fig. 42 FEM Distribution Factor/AASHTO Distribution Factor vs. edge distance for the case with exterior girder, two lanes loaded

5.4.5 Edge Distance

The final variable examined was the edge distance. Edge distances of 0.46 m (1.5 ft), 0.76 m (2.5 ft), 1.1 m (3.5 ft), 1.4 m (4.5 ft), and 1.7 m (5.5 ft), were chosen to cover most of the positive values allowed by the AASHTO LRFD Specifications. After obtaining the distribution factors, the controlling percent differences determined the AASHTO LRFD Specifications to be between 3% and 46% conservative for the single lane loaded, exterior girder case. The exterior girder, two lane loaded case determined the AASHTO LRFD Specifications to be between 24% non-conservative and 17% conservative. Fig. 42 provides the ratio of distribution factors vs. edge distance for the case of exterior girders with a two lanes loaded. For the initial condition of 0.46 m (1.5 ft), the AASHTO LRFD Specifications are non-conservative but as the edge distance

increases, the AASHTO LRFD Specifications become conservative and continue to get more and more conservative. This is also the case for the single loaded exterior girder while the two interior girder cases are approximately the same across each of the edge distances.

CHAPTER 6

SUMMARY AND CONCLUSIONS

6.1 Summary

As part of the Long Term Bridge Performance Program, a live-load test was conducted on a bridge in Perry, UT. A finite-element model (FEM) was created with the same bridge parameters and calibrated based on the live-load test data. The bridge distribution factors determined from calibrated FEM were then compared to distribution factors obtained using equations from the AASHTO LRFD Bridge Design Specifications. Parametric studies on changes in span length, deck thickness, edge distance, skew, and fixity were also conducted in order to determine each of their effects on bridge distribution factors.

6.2 Conclusions

- In all cases, whether it be the comparison of the FEM from the live-load test or the comparison of the FEMs from the parametric studies to the AASHTO LRFD Specification comparison, the single lane loaded, exterior girders controlled.
- The comparison between the FEM distribution factor from the live-load test and the AASHTO LRFD Specifications distribution factor for the controlling case had a percent difference of 55% on the conservative side. In the non-controlling cases, the AASHTO LRFD Specifications were even more conservative by as much as 78%.
- While the range of conservatism was between 55% - 78% when determining the distribution factors using the simply supported moment, when using the moment from a fixed-fixed bridge, the range was between 8% non-conservative and 47%

conservative. This indicates that the bridge falls somewhere in between the two extremes of fixity. The actual fixity was determined to be 94%. In order to provide more adequately sized and economical bridges, the AASHTO LRFD Specification equations need to be adjusted to take into account the fixity of a bridge.

- In every case, the single lane loaded, exterior girder case, was conservative, usually by a wide margin varying from 3% when a variable was taken into account, to 65% when a variable was not taken into account. Because this is the governing case for this type of bridge, the lever rule should be replaced by equations that take into account more of the variables of a bridge, including fixity.
- In the cases of the exterior girder, two lane loaded case, most of the time these distribution factors were non-conservative with respect to the AASHTO LRFD Specification distribution factors. This needs to be modified, especially after changing the lever rule to reduce its conservatism because then this case will control.

6.3 Recommendations for Future Work

Many studies have been done on different types of bridges with integral abutments. In order to provide better equations that take into account the fixity of the bridge for the AASHTO LRFD Specifications, future work could involve compiling these studies and either developing new equations, or developing factors for the old equations for fixity. This would allow for cheaper and more suitably sized bridges by counting on the fixity to reduce the distribution factors.

More studies need to be conducted on the effects of the lever rule on the single lane loaded exterior girder to ensure that the correct equations are being used. This would provide for more economical bridges. In addition a study on the equation for the two lane loaded, exterior girder should also be conducted in order to make it more conservative to prevent non-conservatism.

REFERENCES

AASHTO. (2010). *AASHTO LRFD bridge design specifications*, 5th Ed., American Association of State Highway and Transportation Officials, Washington, D.C.

Barr, P., Eberhard, M., and Stanton, J. (2001). "Live-load distribution factors in prestressed concrete girder bridges." *J. Bridge Eng*., 6(5), 298–306.

Burke, M. (2009). "Integral bridges." *Integral and semi-integral bridges*. Wiley-Blackwell, U.K., 1-19.

Dicleli, M. and Erhan, S. (2009). "Live load distribution formulas for single-span prestressed concrete integral abutment bridge girders." *J. Bridge Eng*., 14(6), 472–486.

Hodson, D., Barr, P., and Halling, M. (2012). "Live-load analysis of posttensioned box-girder bridges." *J. Bridge Eng*., 17(4), 644–651.

Kalayci, E., Civjan, S., Brena, S., and Allen, C. (2011). "Load testing and modeling of two integral abutment bridges in Vermont, US." *Structural Engineering International.*, 21(2), 181-188.

Lahovich, A. (2012). "New technologies in short span bridges: a study of three innovative systems." M.S. thesis, Univ. of Massachusetts Amherst., Amherst, Mass.

Mourad, S. and Tabsh, S. (1999). "Deck slab stresses in integral abutment bridges." *J. Bridge Eng.*, 4(2), 125–130.

APPENDICES

Appendix A

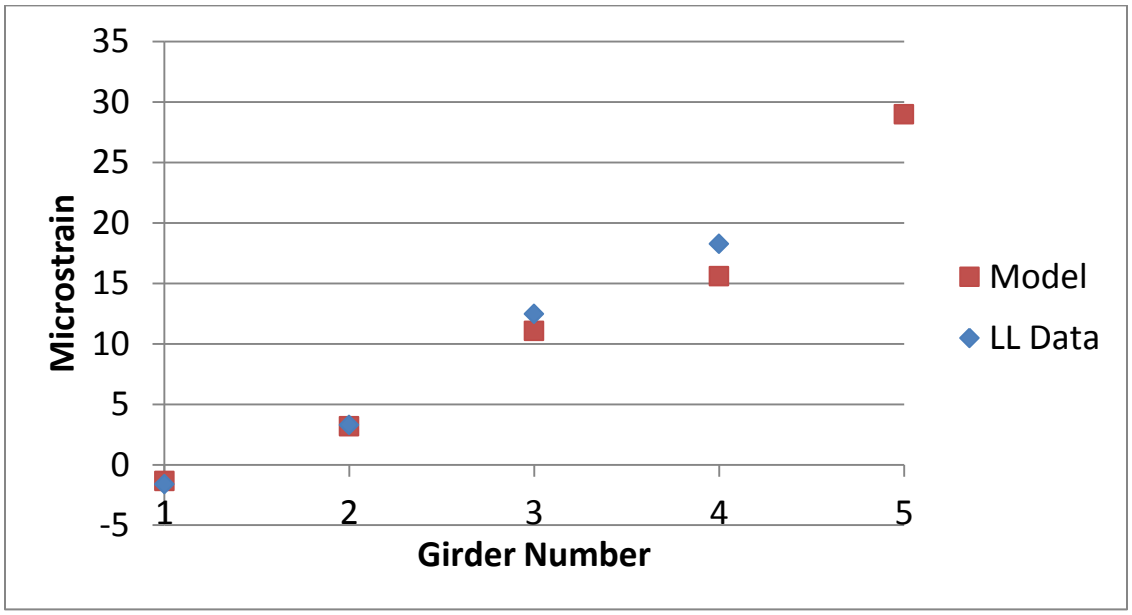

Fig. 43 Microstrain comparison near midspan between live-load data and model for Load Case 4, all girders

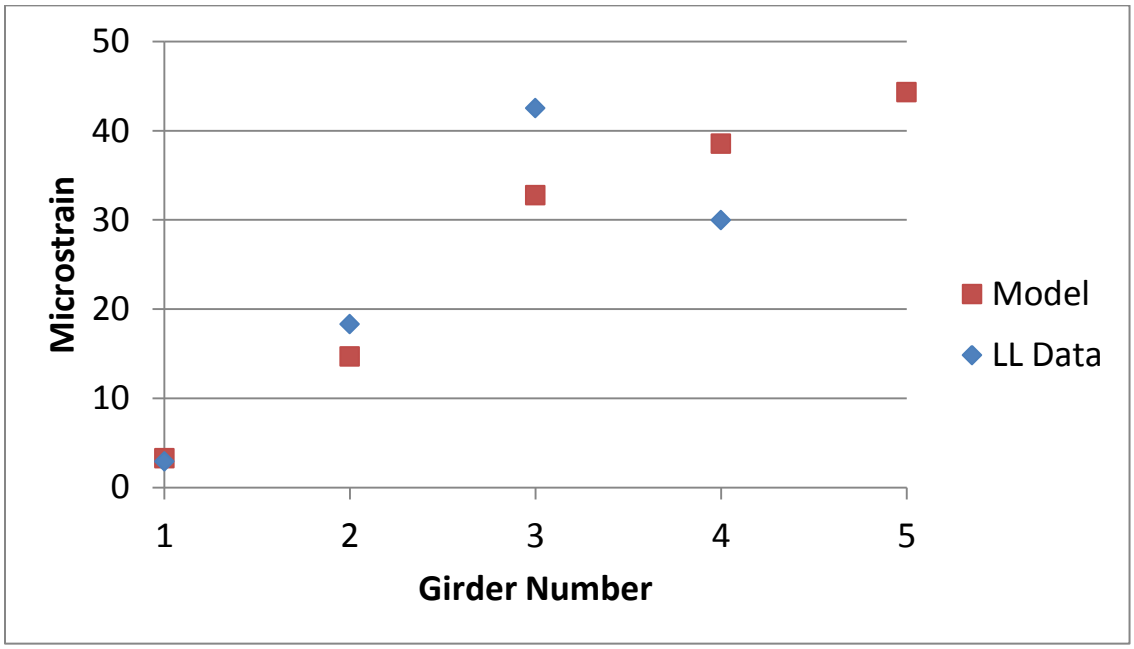

Fig. 44 Microstrain comparison near midspan between live-load data and model for Load Case 2, all girders

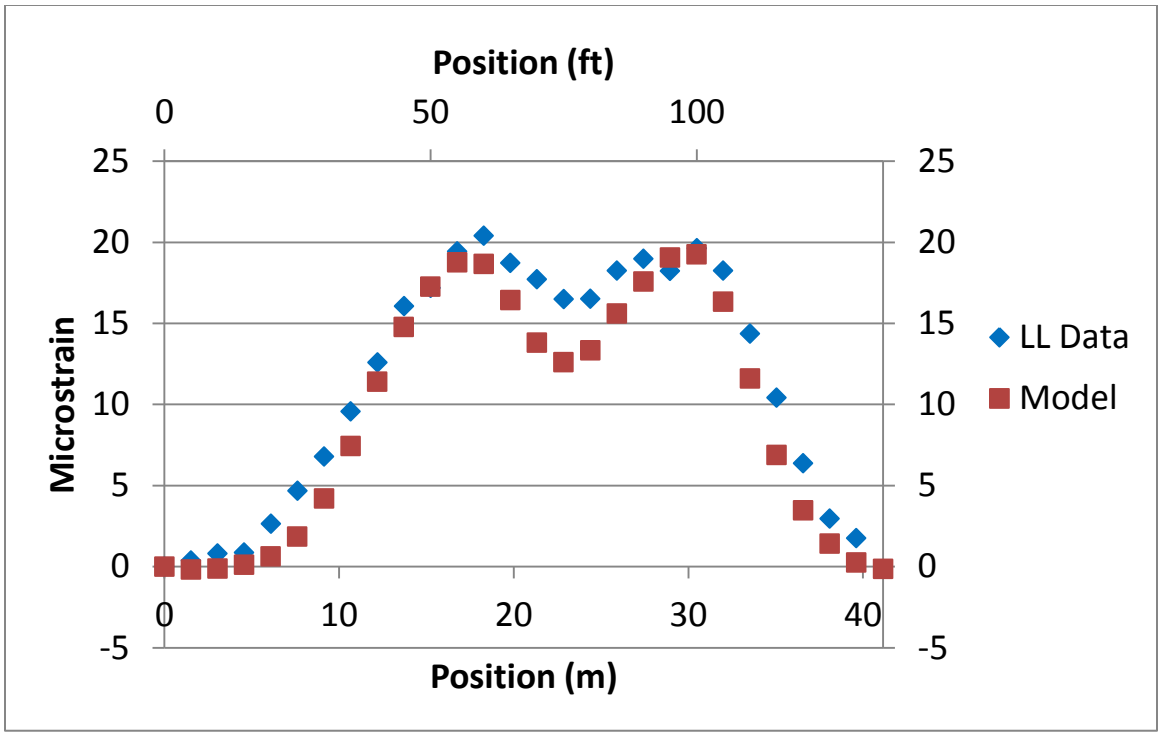

Fig. 45 Microstrain comparison near midspan between live-load data and model for Load Case 4, Girder 4

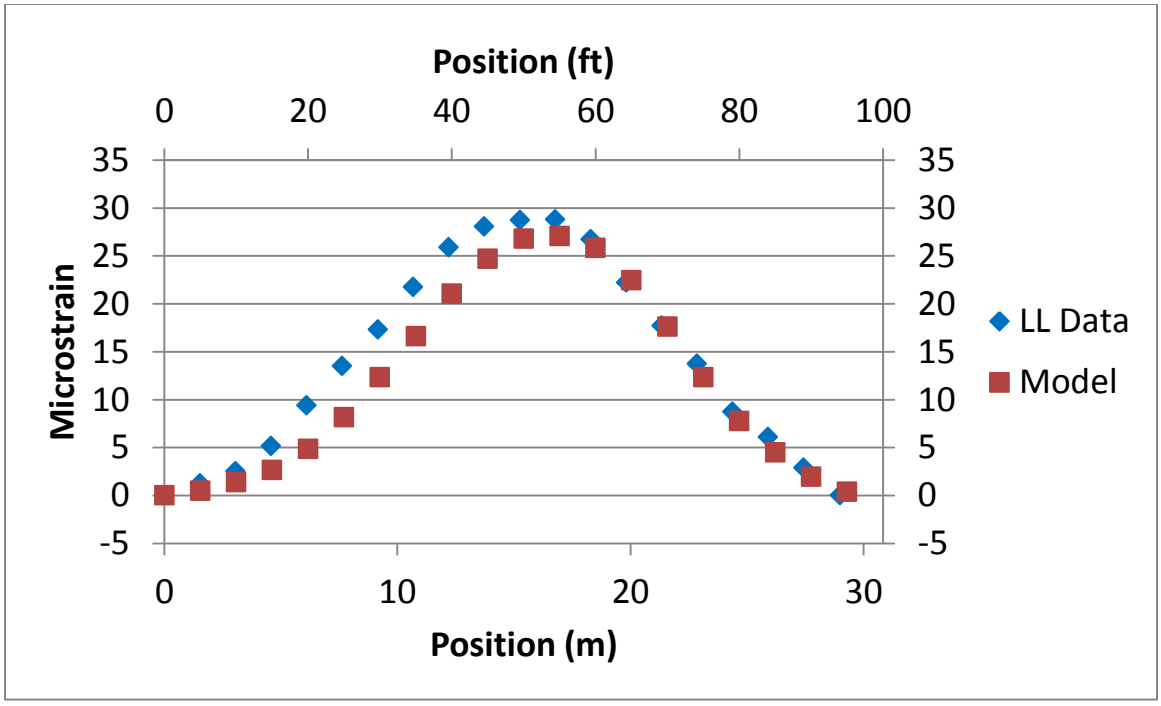

Fig. 46 Microstrain comparison near midspan between live-load data and model for Load Case 3, Girder 1

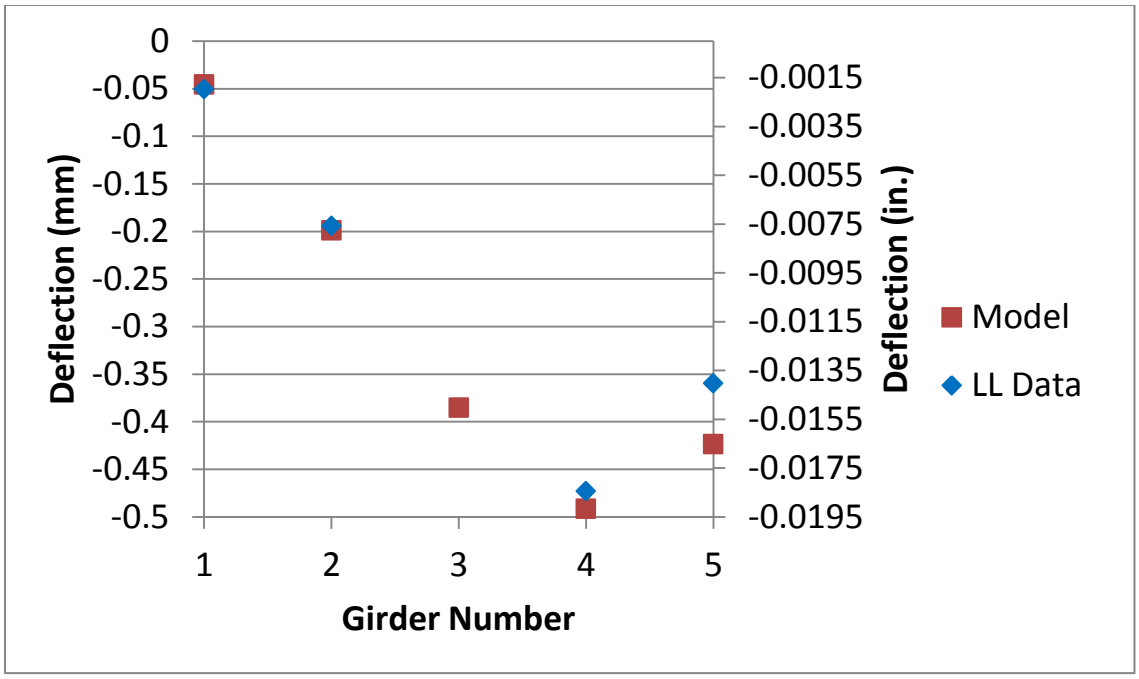

Fig. 47 Deflection comparison at midspan between live-load data and model for Load Case 2, all girders

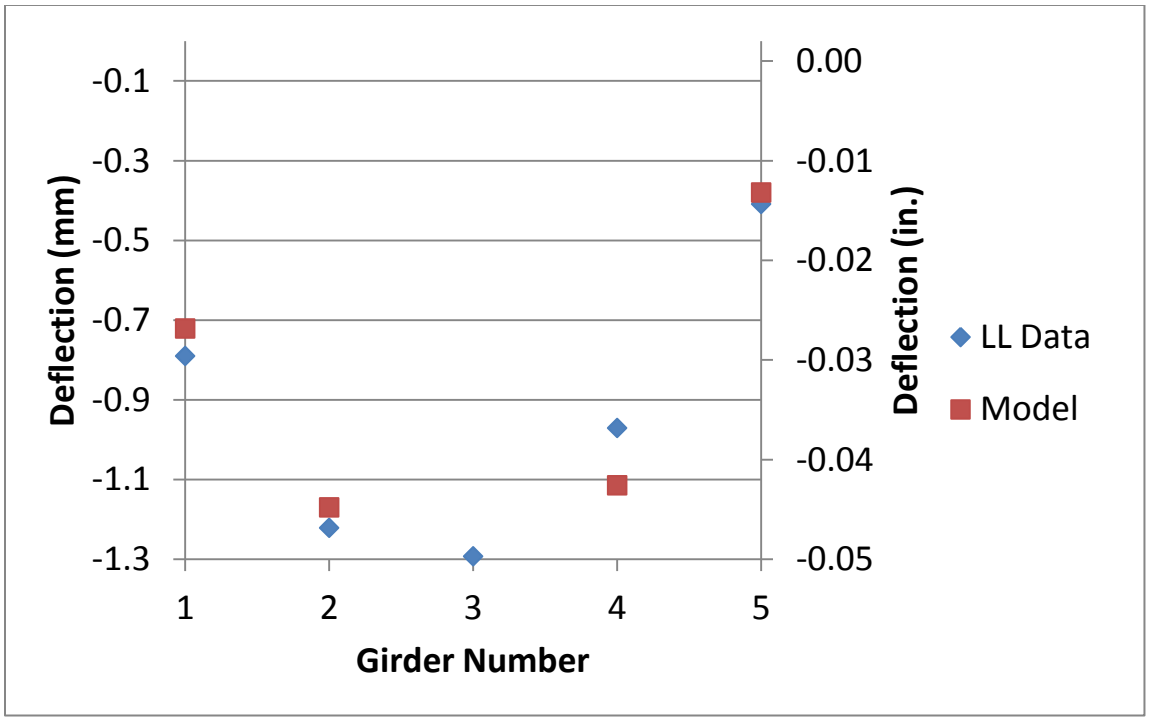

Fig. 48 Deflection comparison at midspan between live-load data and model for Load Case 3, all girders

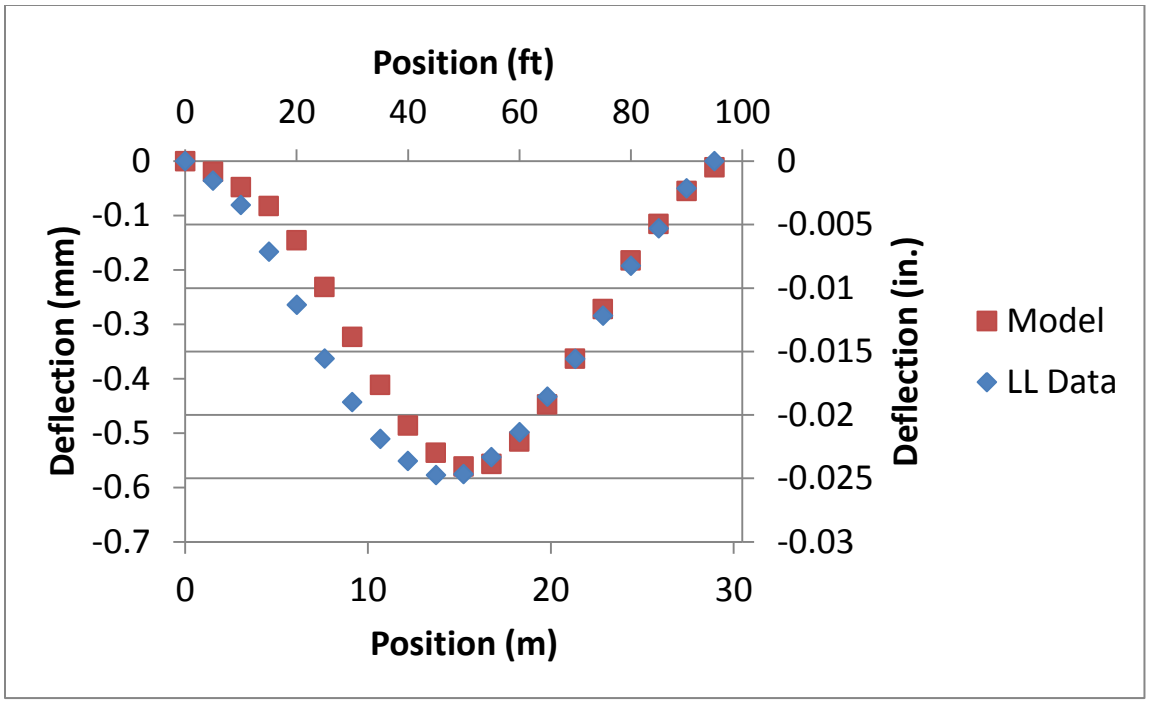

Fig. 49 Deflection comparison at midspan between live-load data and model for Load Case 2, Girder 2

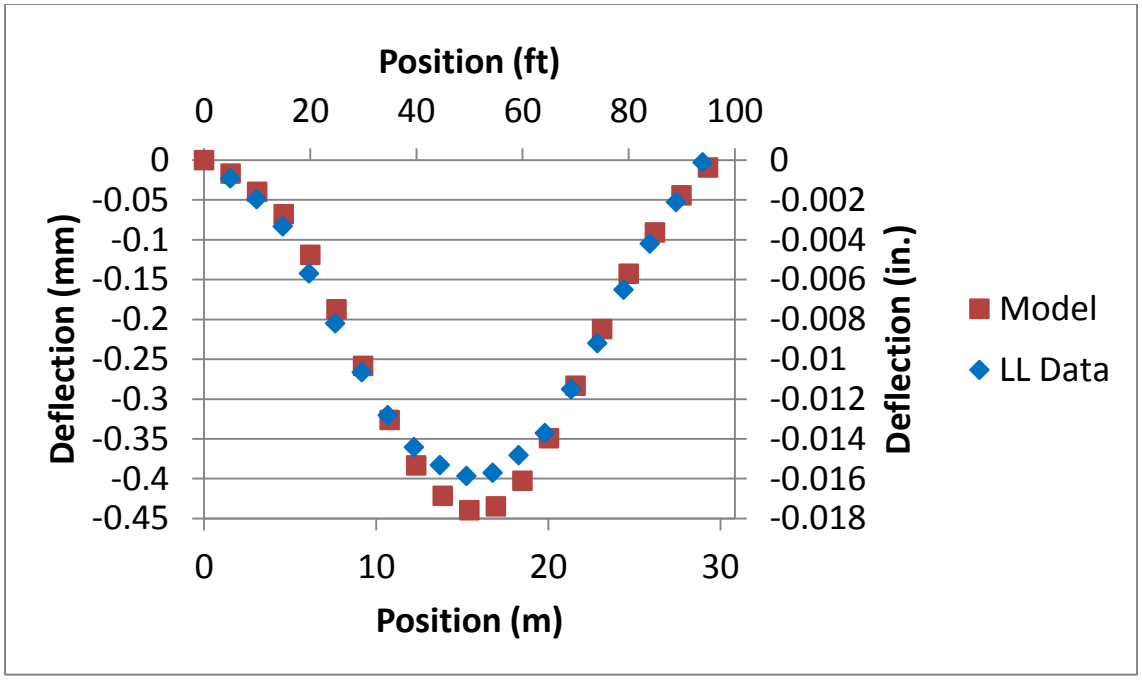

Fig. 50 Deflection comparison at midspan between live-load data and model for Load Case 3, Girder 5

Appendix B

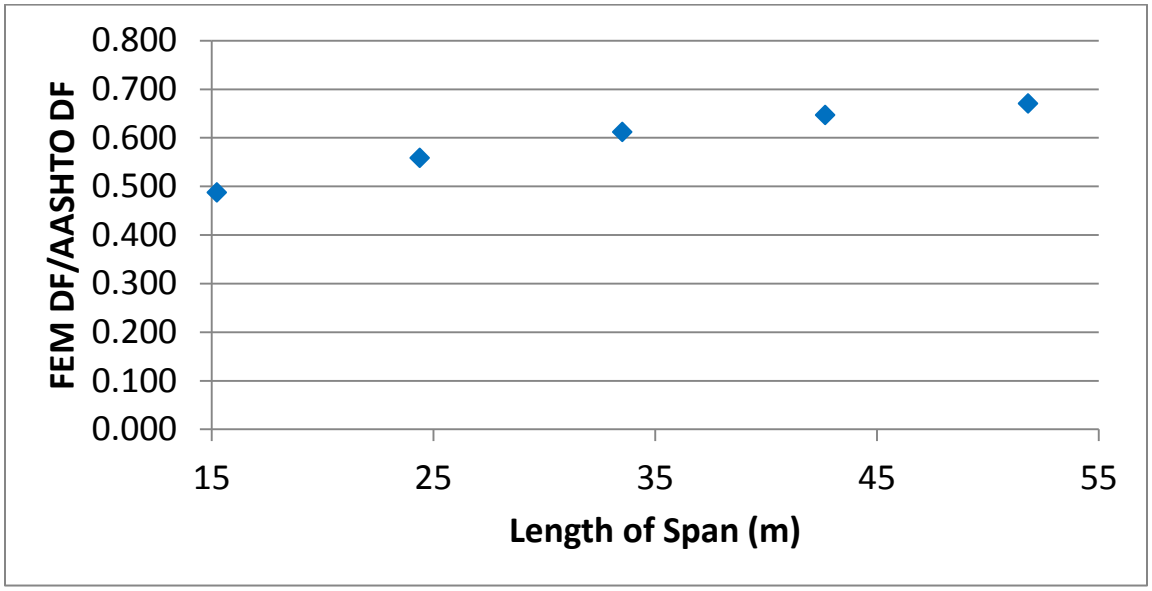

Fig. 51 FEM Distribution Factor/AASHTO Distribution Factor vs. length of span for the case with interior girder, one lane loaded

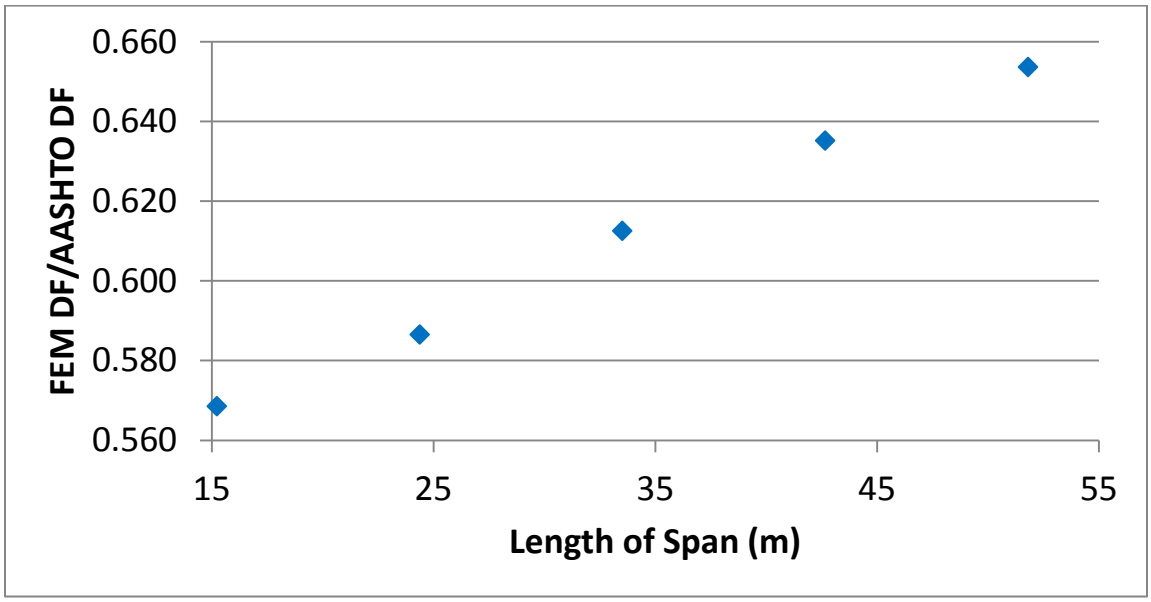

Fig. 52 FEM Distribution Factor/AASHTO Distribution Factor vs. length of span for the case with interior girder, two lanes loaded

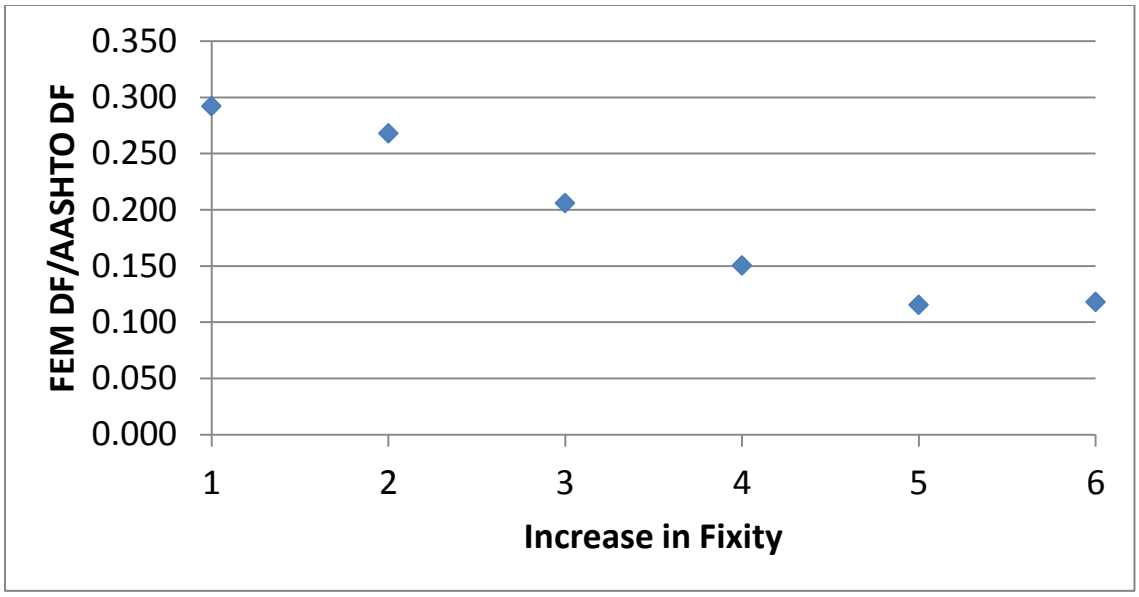

Fig. 53 FEM Distribution Factor/AASHTO Distribution Factor vs. fixity for the case with interior girder, one lane loaded

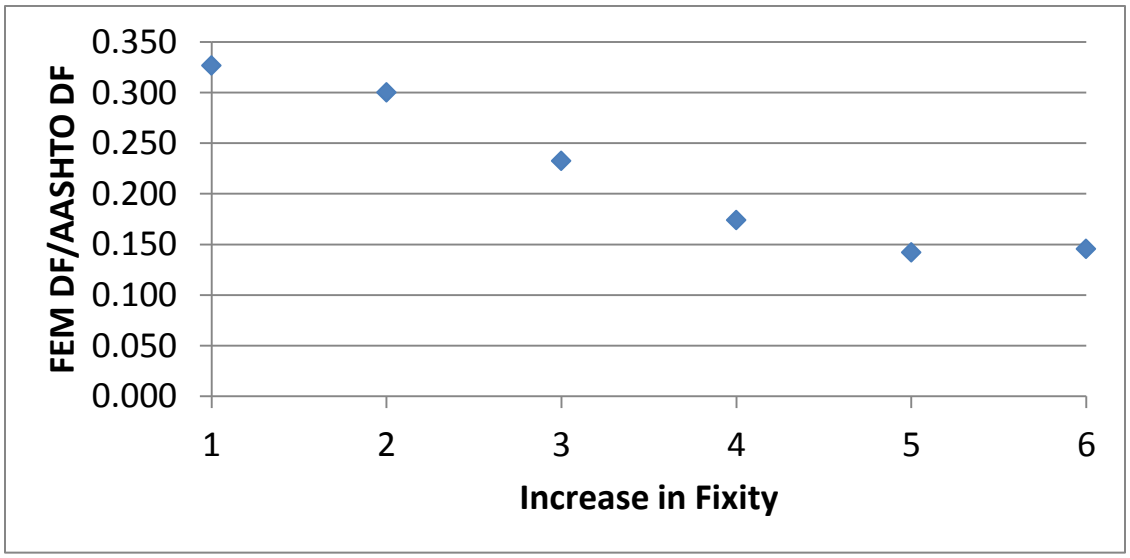

Fig. 54 FEM Distribution Factor/AASHTO Distribution Factor vs. fixity for the case with interior girder, two lanes loaded

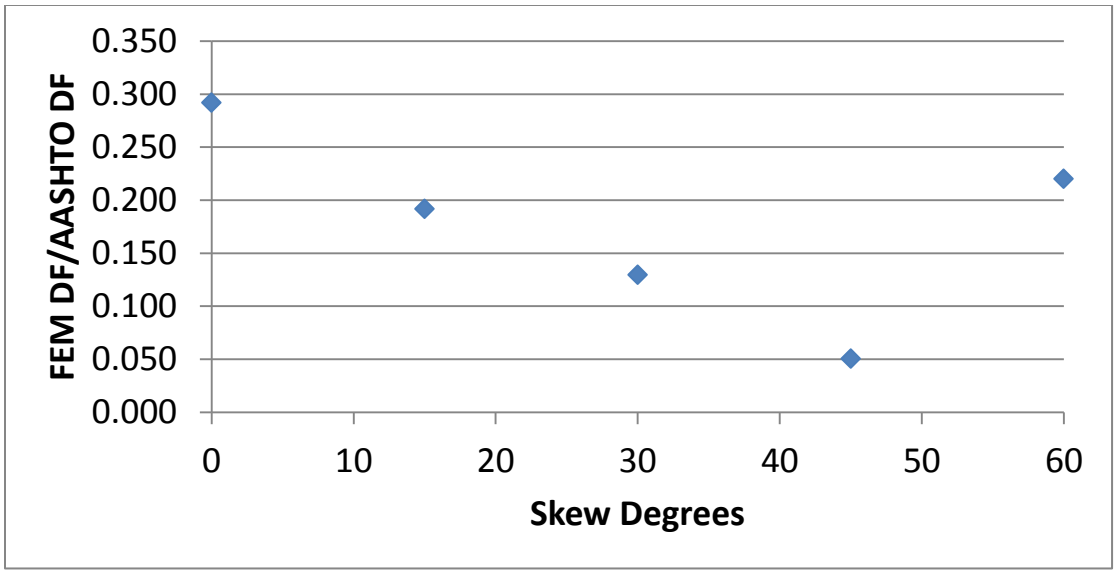

Fig. 55 FEM Distribution Factor/AASHTO Distribution Factor vs. skew degrees for the case with interior girder, one lane loaded

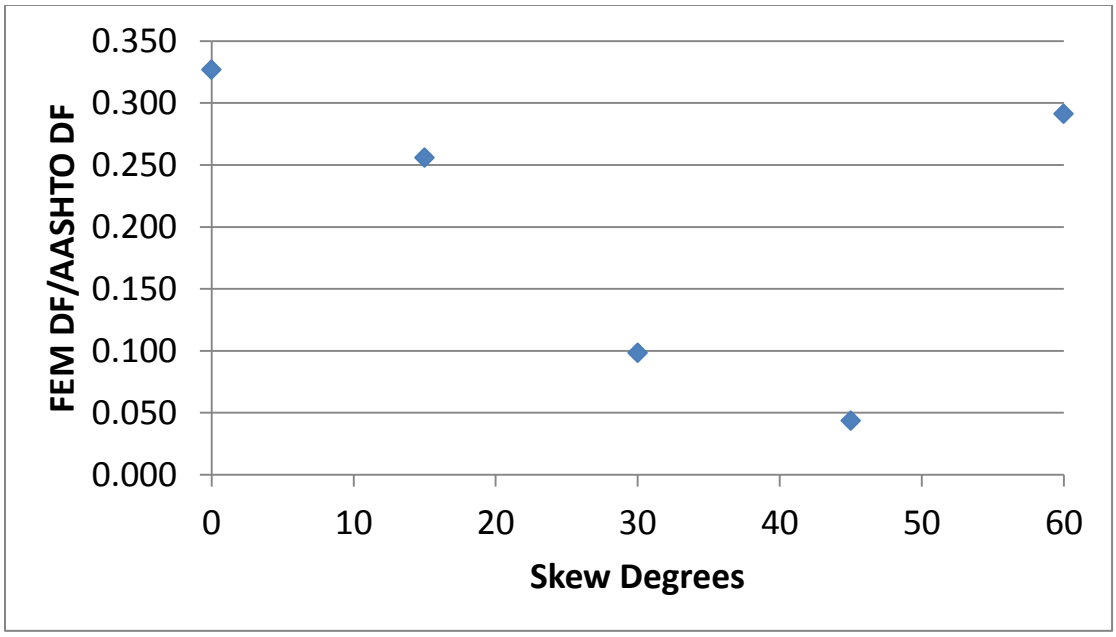

Fig. 56 FEM Distribution Factor/AASHTO Distribution Factor vs. skew degrees for the case with interior girder, two lanes loaded

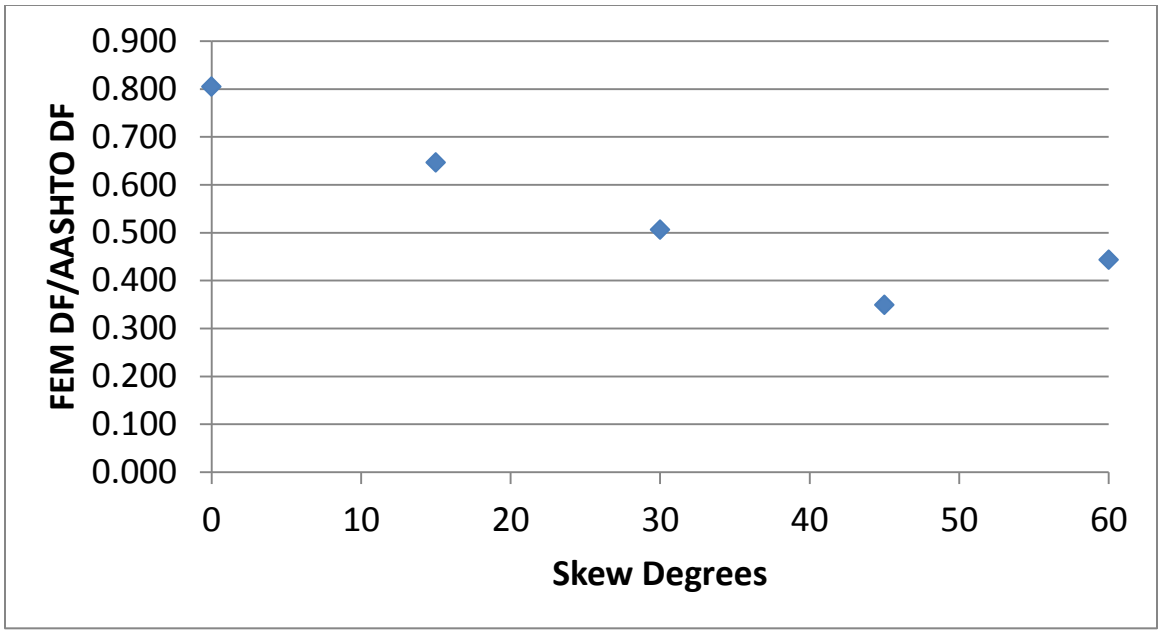

Fig. 57 FEM Distribution Factor/AASHTO Distribution Factor vs. skew degrees for the case with exterior girder, one lane loaded

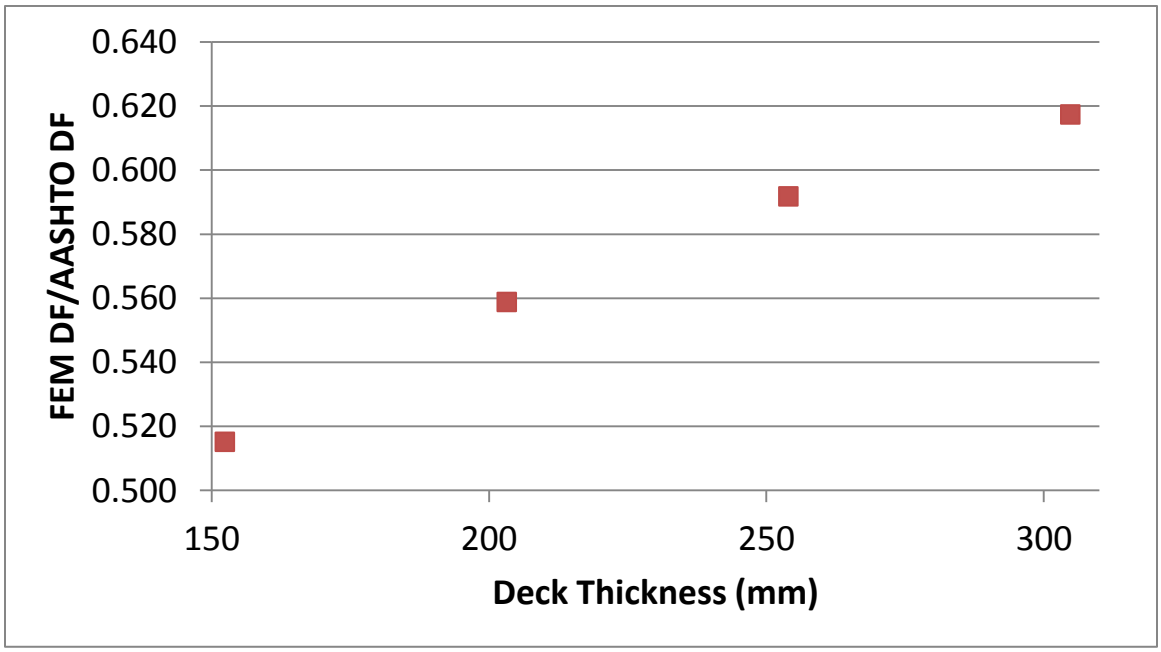

Fig. 58 FEM Distribution Factor/AASHTO Distribution Factor vs. deck thickness for the case with interior girder, one lane loaded

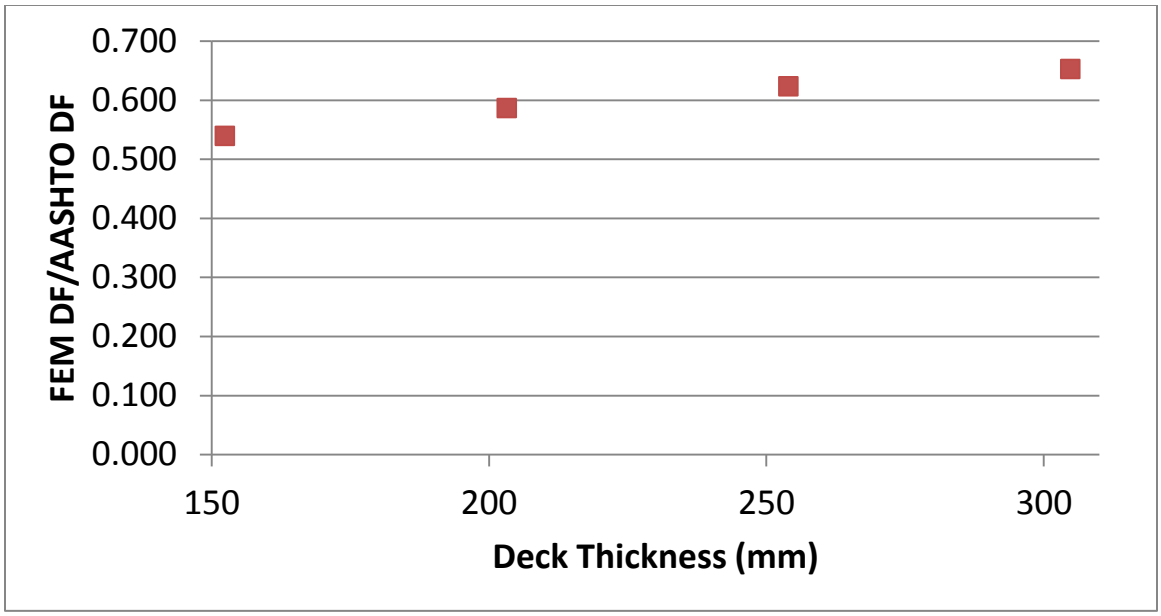

Fig. 59 FEM Distribution Factor/AASHTO Distribution Factor vs. deck thickness for the case with interior girder, two lanes loaded

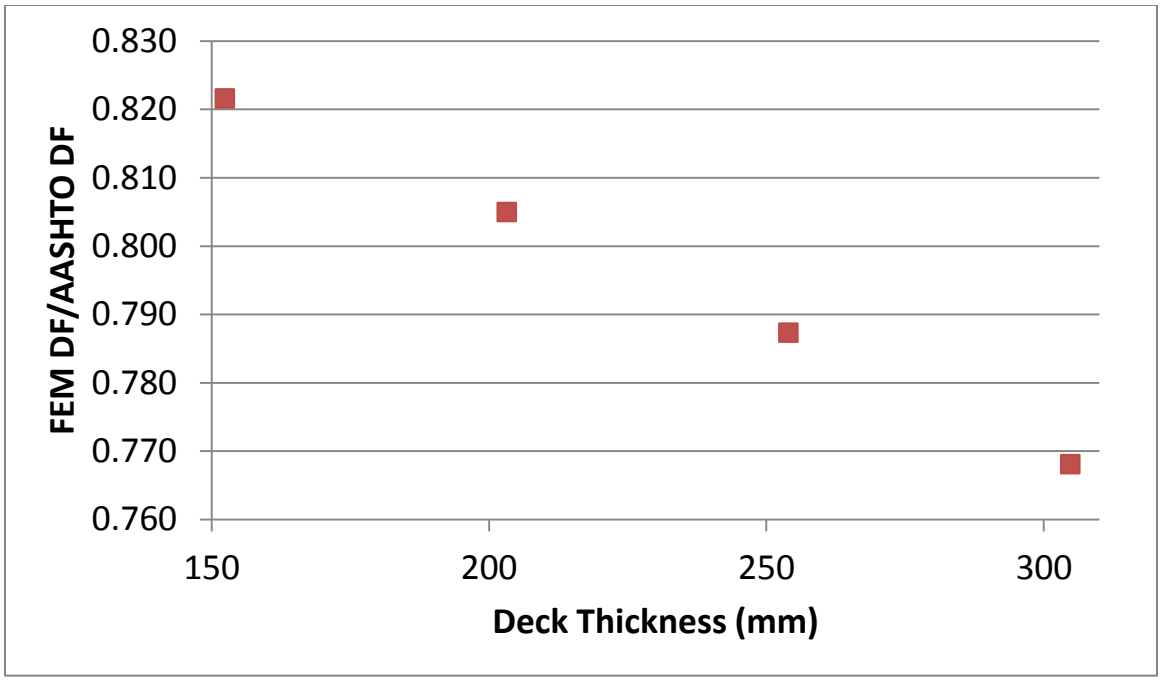

Fig. 60 FEM Distribution Factor/AASHTO Distribution Factor vs. deck thickness for the case with exterior girder, one lane loaded

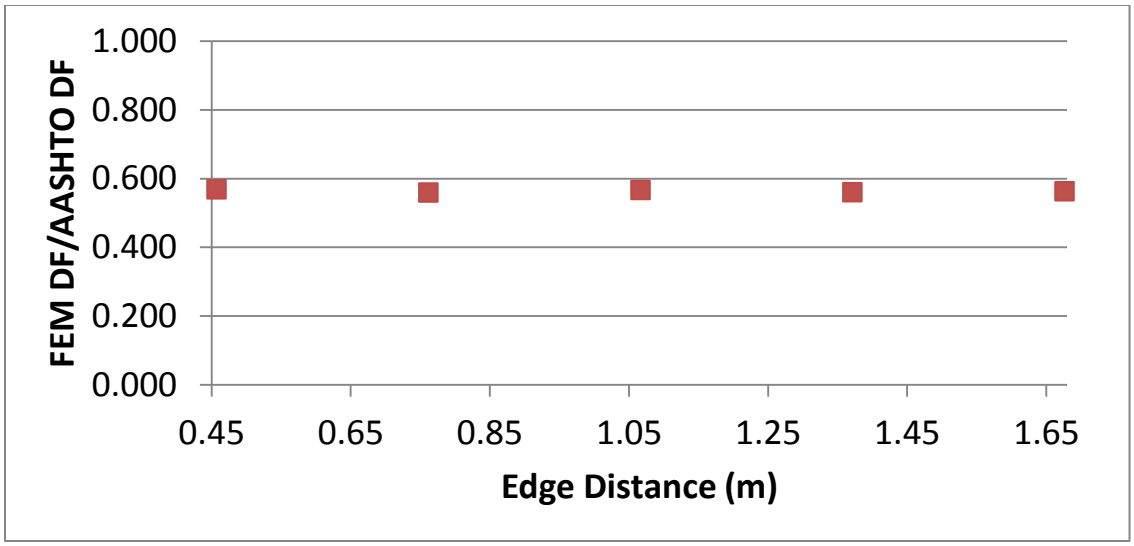

Fig. 61 FEM Distribution Factor/AASHTO Distribution Factor vs. edge distance for the case with interior girder, one lane loaded

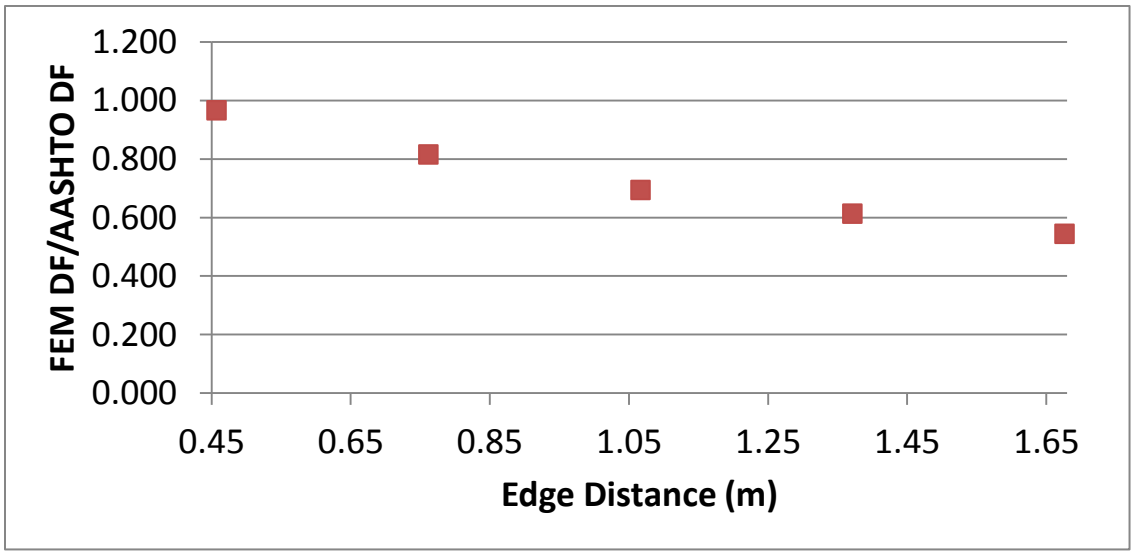

Fig. 62 FEM Distribution Factor/AASHTO Distribution Factor vs. edge distance for the case with exterior girder, one lane loaded

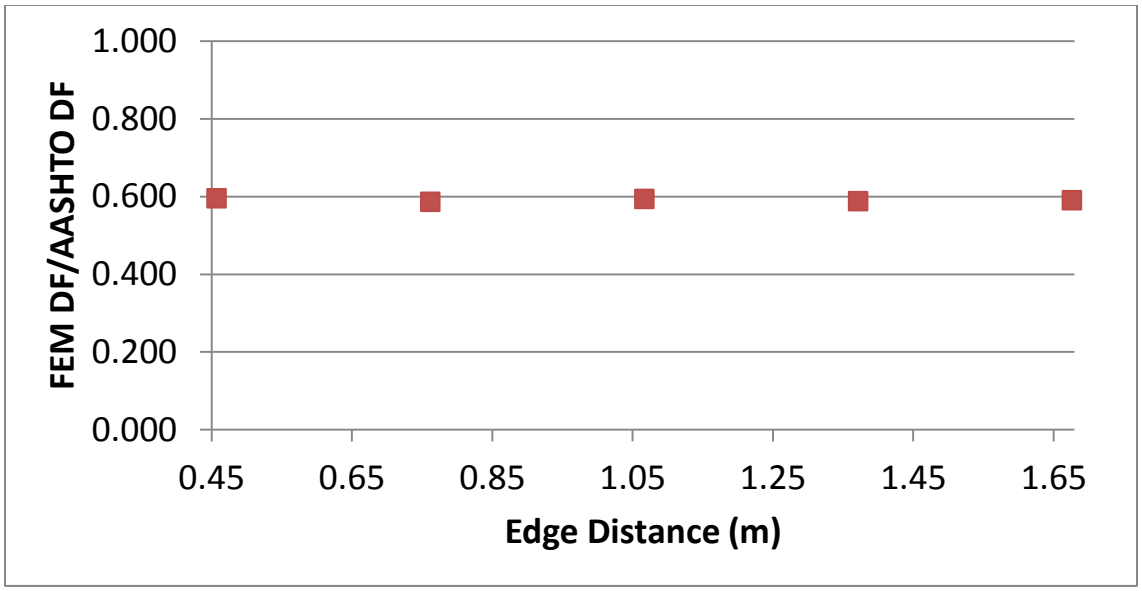

Fig. 63 FEM Distribution Factor/AASHTO Distribution Factor vs. edge distance for the case with interior girder, two lanes loaded